2011

Aging Effect in the Wettability of Nickel Nanorod Arrays

Nahla Albarakati
Virginia Commonwealth University

Aging Effect in the Wettability of Nickel Nanorod Arrays

A thesis submitted in partial fulfillment of the requirements for the degree of Master of Science in Physics / Applied Physics at Virginia Commonwealth University.

By

Nahla Albarakati

B.S. in Physics

King Abdulaziz University, 2004

M.S. in Physics/Applied Physics

Virginia Commonwealth University, 2011

Director:

Dr. Dexian Ye, Assistant Professor, Department of Physics

Virginia Commonwealth University

Richmond, Virginia, 23220

May 9, 2011

Acknowledgments

First and foremost, I am thankful to God for giving me everything, including success in life and in my education. Secondly, I am very thankful to my parents for helping me to become an independent person with a clear vision and a strong faith in myself and in my future. I am grateful that they taught me the importance of education, and constantly encouraged me to work harder and always attempt to do my best. I am equally appreciative towards my siblings, both those who live with me in the USA and those back home, for their love, kindness, care and support.

This thesis would not have been possible without the help of the VCU Physics Department. Sincere thanks goes to my academic advisor Dr. Dexian Ye for his support and guidance. I would like to thank Dr. Alison Baski for aiding me in reaching my full potential. I appreciate her professional mentorship and advice. A special thanks goes to Dr. Maryanne Collinson for her caring, detailed and extremely constructive comments on my thesis. I owe Dr. Dmitry Pestov a debt of gratitude for training me on the SEM and XPS; many thanks to him. I would also like to thank all of my physics professors for their excellent teaching. A warm thanks goes to Janice Guyer and Evelyn Perham for always making me feel welcome and at home. I am grateful for their kindness to me.

I would like to express my thanks and gratitude to everyone in the physics department especially my friends: Iwona, Joy, Rosy, Monika, Joe, Michael, Steven and Aric. I value all of their friendships very much. In particular, I am very appreciative to Joy McNamara and Michael Foussekis for their help in revising and editing this thesis. I would also like to thank all of my incredible friends back home for their love and support, especially Hadeel and Azzah.

I am honored to be graduating from the VCU physics department. Once again, thanks to everyone for their encouragement.

Table of Contents

List of Figures

List of Tables

Abstract

Aging Effect in the Wettability of Nickel Nanorod Arrays

By Nahla Mubarak Albarakati

A thesis submitted in partial fulfillment of the requirements of the degree of Master of Science at Virginia Commonwealth University. Virginia Commonwealth University, 2011.

Major Director: Dr. Dexian Ye, Assistant Professor, Department of Physics

The time-dependent wettability of nickel nanorod arrays was studied by measuring their water contact angles as a function of "aging" time in air. The nickel nanorod arrays were deposited on silicon substrates by DC magnetron sputtering using an oblique angle of 85° with respect to the substrate normal. By changing the deposition time from 10 to 90 min., the diameter, height, and separation of the nanorods were varied. The water contact angles of each sample were then periodically measured from a minimum aging time of 30 min. after deposition and exposure to air, up to a maximum aging time of three months. The initial water contact angles for all samples were approximately equal to 8o, indicating that the nickel nanorod arrays were initially superhydrophilic. As the samples aged in air, however, they all showed increasing contact angles as a function of time that were nonlinear with different rates. The results can be grouped into two categories: thinner samples with shorter deposition times (10 to 55 min) demonstrated faster rates of increase in contact angle, and thicker samples with longer deposition times (60 and 90 min.) showed slower rates. The increase in contact angle with time indicates that the Ni nanorods become more hydrophobic with aging time in air. Surface chemical analysis demonstrates that this increase in hydrophobicity may be due to oxidization and hydrocarbon

contamination, which depend on the nanorod morphology. X-ray photoelectron spectroscopy results indicate that thinner samples (10-55 min. deposition time) have more adsorbed carbon as compared to thicker samples (60 and 90 min.). It appears that the reactivity of the Ni nanorods with air ambient is enhanced for shorter, smaller-diameter nanorods.

Chapter 1: Wetting

1.1 Introduction

Wetting is the ability of a liquid to extend over a solid surface, keep contact with it, and form a continuous film. Wetting occur when there is a strong attraction between the solid and liquid at the interface. Two types of forces control this interaction, and determine the degree of wettability: adhesive and cohesive forces.[1] In order for the liquid to wet a surface, the adhesive forces between the liquid and solid should be greater than the cohesive forces of the liquid itself. Otherwise, wetting will not occur. Experimentally there is a simple technique to quantify the wettibility of a liquid on a solid surface, which is the contact angle measurement. The contact angle is the angle between the solid-liquid interface and the liquid-vapor interface of a sessile drop of liquid sitting on the solid surface.

There are two kind of solid surfaces in terms of solid-liquid interactions: high surface energy and low surface energy. The high surface energy solids disperse the liquid completely upon contact. Low energy surfaces have either complete or partial wetting. A 0° contact angle can be observed if the solid-liquid interaction is in a state of complete wetting. For partial wetting states, a finite contact angle between 0° and 180° can be measured on the surface. If the liquid has a lower surface energy than the solid, then the surface becomes more wettable with small contact angles. On the other hand, if the liquid has a higher surface energy than the solid, the surface will not achieve complete wetting.

The contact angle and the surface energy are related by the empirical Young's equation. This equation is based on ideal solid surfaces which are flat, dense, and chemically homogeneous. The contact angle of a liquid that partially wets the surface follows Young's equation: [2]

$$\cos\theta_E = \frac{\gamma_{SV} - \gamma_{SL}}{\gamma_{LV}} \tag{1}$$

where θ_E is Young's contact angle, γ_{SV} is the interfacial tensions (or surface energy) between the solid and the vapor, γ_{SL} is the interfacial tensions (or surface energy)

between the solid and the liquid and γ_{LV} is the interfacial tensions (or surface energy) between the liquid and the vapor.

In an experiment, the measured water contact angle is the angle formed by two tangent lines at the liquid-air interface and the liquid-surface interface, respectively. If the value of the water contact angle θ is between 0° and 90°, the water will spread over a large area and the surface will become wetted. Conversely, if the value of the water contact angle θ is between 90° and 180°, the water will only spread over a small area and the surface will be defined as non-wettable. A water wettable surface may be called hydrophilic surface, and non-wettable surface hydrophobic surface.

The water contact angle changes depending on the surface energy and the roughness of the surface.[2, 3] The roughness of a surface can be modified by several methods, for example by chemical etching and thin film coatings. In thin film deposition, the roughness varies with growth process and deposition techniques. Changing the deposition time of samples gives surfaces with varied roughness.[4]

The effect of surface roughness on the wettability has been described by two models: the Wenzel model and the Cassie-Baxter model.[2] In the Wenzel model, it is assumed that the hollows of the rough surface are filled with liquid. Wenzel argues in his theory that a rough surface has a higher surface area than that of a smooth surface. Thus, the surface energy in the rough surface is greater than that of a smooth surface. The relationship between surface roughness assuming a chemically homogeneous surface and the contact angle is given by the following equation: [5, 6]

$$\cos\theta_W = r\cos\theta_E \tag{2}$$

where θ_W is the apparent contact angle at a rough surface in the Wenzel model, while θ_E is Young's contact angle and *r* is the roughness factor. The size of the rough features needs to be approximately the size of the droplet or smaller.

In the Cassie-Baxter model, a rough surface is described as a chemically heterogeneous surface. A heterogeneous surface implies that the surface is composed of at least two types of species. Each species will have a unique contact angle. An important factor to take into account is that the rough surface could be composed of the air and the

solid. According to this model, the surface can have air gaps between the extrusions on the rough surface. The equation that describes the Cassie and Baxter model is shown below: [4, 7]

$$\cos\theta_{C_B} = f_S \cos\theta_S - f_V \quad (3)$$

where θ_{C_B} is the apparent contact angle in the Cassie-Baxter model, f_S is the surface area of solid-water interface and f_V is the surface area of water-air interface; θ_S is the solid-water contact angle. Again in this model, the drop size must be larger than the roughness features.

1.2 Literature Review

It has been noticed that on metallic surfaces the water contact angles change with time when metals are vacuum deposited. This phenomenon is referred as "aging effect" of the contact angle. The water contact angles of gold and silver films were studied by Bartell and co-workers in 1941.[8] The samples were prepared in vacuum by vaporizing the metals on polished Pyrex glass tips. The samples were perfect mirror surfaces with both silver and gold coatings. Bartell *et al.* used the sessile drop method to measure the contact angles of water in a sequence of time. In less than a day of air exposure, they observed that the advancing contact angles on these two metals changed from hydrophilic to hydrophobic. In a period of about 18 hours, the advancing contact angle of gold surface changed from 40° to 95°, and for silver surface from 37° to 92.5°. They argued that the reason for this change was the contamination of the air. The contact angle was small when the samples were freshly prepared before any contamination. As the metals were exposed to the air, they adsorbed species from the air. The result was an increasing contact angle. However, they believe that the oxidation of the surface was not the reason for the increasing contact angles, because oxidized metals are more hydrophilic than pure metals.[8]

Another study was done by Trevoy and Hollister in 1958.[9] In this study various metals or alloys had decreasing contact angles after a special treatment. This process included chemical cleaning with strong oxidizing acids, electropolishing and handling

techniques. As a result, the substrates not only became clean and free of contamination, but also had smooth surfaces. With this kind of surface, they avoided the complication of surface roughness in the contact angles measurements. The process was able to remove all organic matter that could cause an increase in the contact angle. The metals or alloys used in the study were aluminum, brass, copper, magnesium, nickel, stainless and zinc. They also used the sessile drop method to measure the water contact angles. For advancing contact angles, they found that the contact angles were varied in the range from 0° to 10.5°.[9] They attribute this large variation in values to the adsorption of organic molecules from the air. The angles were unique for each metal, depending on its ability to absorb impinging organic molecules.[9]

To the best of our knowledge, there is no report in literature about the changing of contact angles on nanostructures surfaces with time. In this thesis, we will study the aging effects on the wettability of nickel nanorod arrays by measuring the water contact angles for each sample. Nickel nanorod arrays were fabricated on silicon substrates by the oblique angle sputtering deposition. Various deposition times for samples used in this study were 10, 20, 30, 45, 50, 55, 60 and 90 minutes in order to grow nanorods with different heights. By measuring the water contact angles, we can study the wettability and the aging effects of these surfaces. The data was taken over the span of approximately three months.

Chapter 2: Experiments

2.1 Sample preparation

Vertically aligned nickel nanorod arrays were deposited on silicon substrates by sputtering at an oblique angle. Oblique angle deposition changes the direction of the arriving vapor to an off-normal direction, which is different from normal thin film deposition.[3,4,10] In our deposition system, the vapor deposits on the substrate at a glancing angle of $\theta = 85°$. The glancing angle θ is measured between the substrate normal and the direction of the incident vapor flux. A silicon substrate was fixed on a sample holder which was rotated by a stepper motor. The substrate and the holder were tilted in such a direction to create the value of the glancing angle that was chosen, i.e. $\theta = 85°$. This setup is schematically shown in Fig. 2.1. The sample was rotated at a speed of 0.5 revolutions per second (rps) during the deposition.

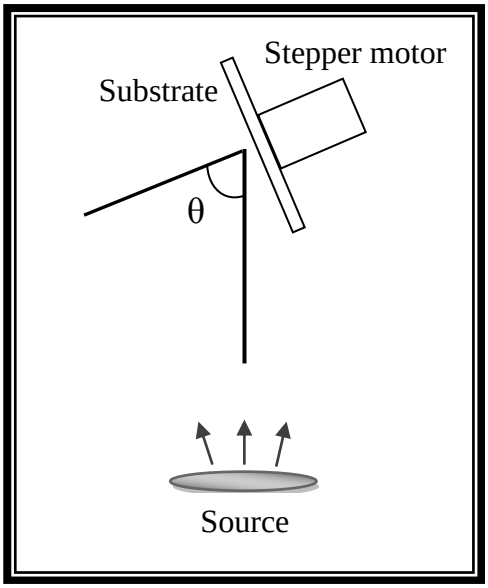

Fig. 2.1: Oblique angle deposition's technique.

Sputtering is a physical vapor deposition (PVD) process where atoms from the source are ejected due to bombardment with energetic ions. The sputtering process used in this study is a direct current magnetron sputtering which is a pliable technique used to deposit a thin film of atoms onto a substrate.[11] The deposition chamber was evacuated by a turbo pump system to a base pressure about 1.7×10^{-7} Torr. Once the chamber achieved

this high vacuum level an argon gas was introduced into the chamber through a control valve. The minimum argon pressure needed to generate the plasma is about 2.5 mili-Torr. A DC voltage was applied between the target and substrate to create the plasma and accelerate the ions toward the target. The sputtering power was 200 Watts. Atoms are ejected when the energy of the argon ions is greater than the surface binding energy of target. Electrons and argon ions are confined close to the target by the magnetic field from the magnet that was placed behind the target. The whole unit of target with its holder and the magnet is called magnetron. The advantages of confining the electrons and argon ions close to the target are increase the sputter rate and reduce the damage to the deposited film.

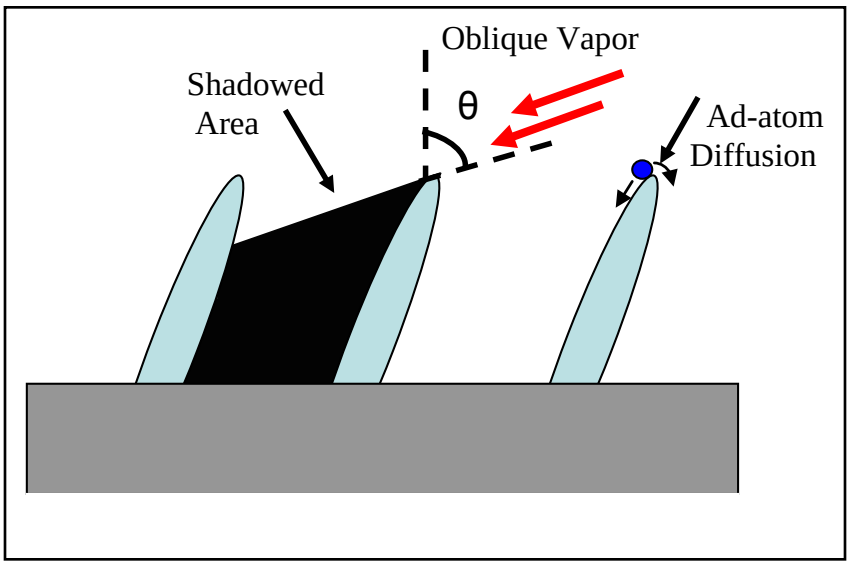

Fig. 2.2: Mechanisms of nanorods growth.

The main mechanisms of generating nanorod arrays are the ad-atom diffusion and shadowing effect in oblique angle deposition.[3] At large incident angle of the incident flux, the atoms deposited on the substrate create shadowed areas behind them. Shadowed area prevents other atoms to reach it. Therefore the film stops growing in these areas, as shown in Fig. 2.2. The arriving vapor had the same direction all the time of deposition which caused the atoms deposited almost in the same area to build the nanorod. If the substrate is kept at rest, the resulted nanorods will incline towards the source of the deposition flux. By rotating the substrate during the deposition, the nanorods are aligned vertically on the substrate. For nickel nanorods, the surface diffusion of atoms promotes

the newly deposited atoms to move on the surface and find an energetic favorable site to settle down. This diffusion process is limited by the lower kinetic energy of the incident atoms. Therefore, the nanorod morphology can be preserved. As such, individual nickel nanorod grown in our technique is a single crystal. Furthermore, the crystalline nature of nickel gives nanorods tip structure as shown later in SEM images at chapter 4.

We prepared nickel nanorod arrays with different heights for the study of water wettability, where the height was controlled by the deposition time. We made totally eight samples; each sample has different deposition time, 10, 20, 30, 45, 50, 60 and 90 minutes. We repeated the experiment with second set of samples have similar deposition time and added one more sample with time deposition of 55. At this second set of samples the distance between the source and substrate during the deposition was longer comparing to the first set of samples. This change causes a difference in the structure parameters of nanorods between the two sets, which is clarified in chapter 4. However our studying of wetting is based on nanorods heights. After deposition was completed, we waited until the chamber cooled down before removing the sample.

2.2. Water Contact Angles Measurement

The water contact angles were measured by using the sessile drop method applied in contact angle goniometer (Rame-Hart Instrument Co.) that has optical subsystem to capture the image of a water droplet on a substrate, shown in Fig. 2.3. The first measurement was taken immediately after removing the sample from the chamber, with around 30 minutes air exposure time; and the rest of measurements were at various aging time periods over three months in air. The procedures used to measure the water contact angles were first turn the power on for all goniometer sets. Then the sample is placed on the stage. After the drop is dispensed from the tip, the tip is slowly moved down toward the surface. When the droplet touches the sample, the tip is quickly moved up and a picture taken immediately. The volume of droplets of de-ionized water that was used for all samples is 3 μL. The tip is always fixed at the same distance away from the stage for all samples. Every droplet was placed on different spots on the sample surface. Some

spots may have been reused after the previous experiments were completely dry in order to study the effect of the water damage to the surface.

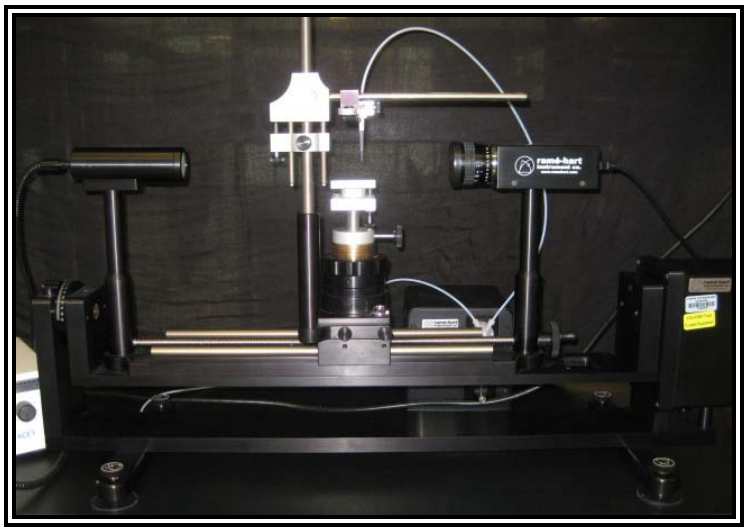

Fig. 2.3: Contact angle goniometer for measuring contact angle.

The water contact angle is measured from the images by using a special program called Image-J, which is public-licensed software and downloaded from the Website of the National Institute of Health at http://imagej.nih.gov/ij/download.html. The image of the droplet was opened via this program, and then the angle was measured by using an angle tool as shown in Fig. 2.4. The water contact angle is the angle between the solid-liquid interface and liquid-vapor interface. For each droplet the measurement of angle was taken several times then the average was calculated.

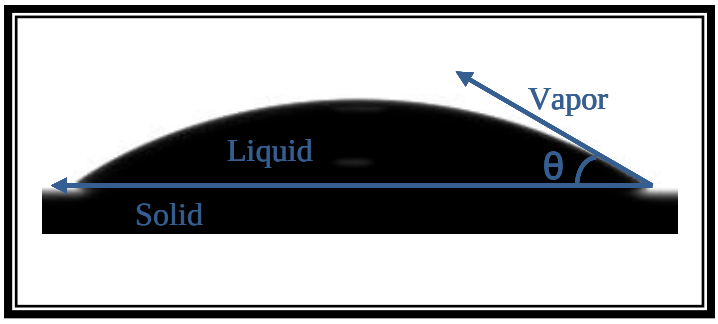

Fig. 2.4: Measurement of water contact angle on nickel nanorod arrays.

2.3. Morphology Analysis

A Scanning Electron Microscope (SEM) (Hitachi FE-SEM Su-70) was used to study the microstructures for all the nanorod array samples. SEM is a microscope which uses a beam of electrons to scan the sample, and obtain an image. The energy value of the electron beam applied to our samples was 5 KeV. A beam of electrons produced in the electron gun at the top of the microscope by the field emission method. These electrons are then passed through electromagnetic lenses before reaching the sample. The distance between the objective lens and the sample was about 7 mm. By taking top view and cross sectional images, we know the approximate height, diameter and the separation between the nanorods. By making a threshold cut-off to the top view SEM images through the Image-J program, the diameter and separation were measured. From cross section SEM images, the height of nanorods was also measured using the Image-J program. Each reported value is the average of several measurements. These parameters were used to find the roughness ratio for each sample, and therefore to study the water contact angle changes with surface roughness.

The roughness ratio *r* is the ratio of real area of nanorod surface compared to the apparent area. According to the SEM images, there are two shapes of nanorods, depending on the heights of the nanorods. The first one is assumed to be a cylindrical shape with smooth end surface for the nanorods of samples with 10, 20 and 30 min deposition. From the SEM cross-sectional images, the tip structure cannot be identified for these films. The roughness ratio *r* becomes: [3]

$$r = 1 + \frac{\pi D h}{L^2} \tag{4}$$

where D, h and L are the diameter, the height and the separation between nanorods, respectively. The second type of nanorods develops a clear tip structure in the SEM cross-section images. Therefore, the top of the rod and the base of the rod are assumed to be a cone and a cylinder, respectively. For a simple approximation, we can assume the angle of the tip of the cone is 90°. The real area of the nano rod includes the area of cylinder, the area of cone and apparent area, L, without the base area of cylinder. We can write the roughness ratio *r* based on the geometry schematically drawn in Fig.2.5:

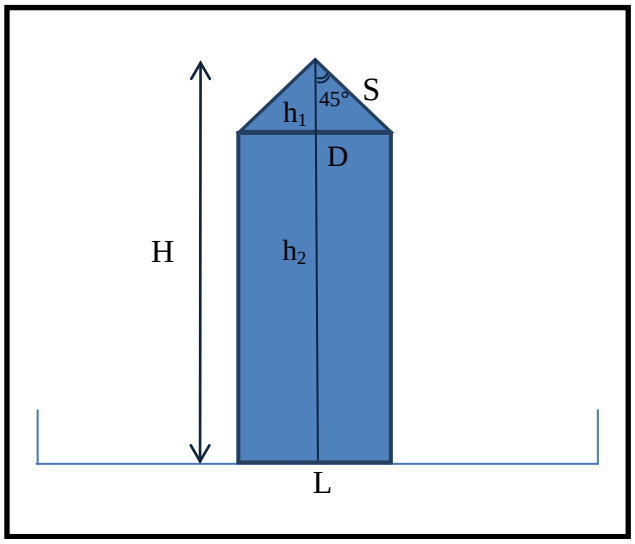

Fig. 2.5: Schematic of nanorod to find the roughness ratio.

Real area:

$$= \left[L^2 - \pi \left(\frac{D}{2}\right)^2\right] + \pi D\, h_2 + \pi \left(\frac{D}{2}\right) S$$

$$= L^2 - \pi \left(\frac{D}{2}\right)^2 + \pi D \left(H - \frac{D}{2}\right) + \pi \left(\frac{D}{2}\right)\left(\frac{D}{\sqrt{2}}\right)$$

$$= L^2 + \pi D \left(H - \frac{D}{4}\right) + \frac{1}{\sqrt{2}}$$

So, the roughness ratio *r* equation becomes:

$$r = \frac{L^2 + \pi D \left(H - \frac{D}{4}\right) + \frac{1}{\sqrt{2}}}{L^2}$$

$$r = 1 + \frac{\pi D\,(H - 0.4D)}{L^2} \qquad (5)$$

2.4. X-ray Photoelectron Spectroscopy

X-ray photoelectron spectroscopy (XPS) is a very surface sensitive technique. XPS was used in our experiment to analyze the change of surface chemical composition of the samples over aging time in air. We performed the XPS measurements at three different times. For the first measurement, we performed XPS experiments when the samples were fresh prepared and just removed from the chamber, about 30 minutes exposing to air. The remaining measurements were performed after one month and two months.

XPS is based on the photoelectric effect. By irradiating X-rays upon the surface, photoelectrons escape from the surface. The detector collects these photoelectrons, and counts them depending in their kinetic energy. The kinetic energy is related to the original elemental orbital of the photoelectrons, which has a unique value of binding energy.

The XPS data were collected in a Kα X-ray photoelectron spectrometer (Thermo Scientific) using a monochromatic Al Kα X-ray source with photon energy of 1486.6 eV. The pass energy for the analyzer energy CAE mode was 150 eV for the survey scans, and 20 eV for the high resolution scans. The X-ray beam arrives at 45° off-normal to the sample, while the detector is normal to the sample. The pressure of analysis chamber was 9×10^{-9} Torr. The percentage of atomic concentrations of detecting elements was calculated to make the comparison between the samples over aging time in air. The calculations based on the peak areas that are given from the program and atomic sensitivity factors from known certified standards.

Chapter 3: Water Contact Angles

3.1 Wettability over Aging Time in Air

Figure 3.1 (a-d) shows some representative images of the water droplets on the sample surface. This series of images illustrate how the contact angle changes with aging time for all samples.

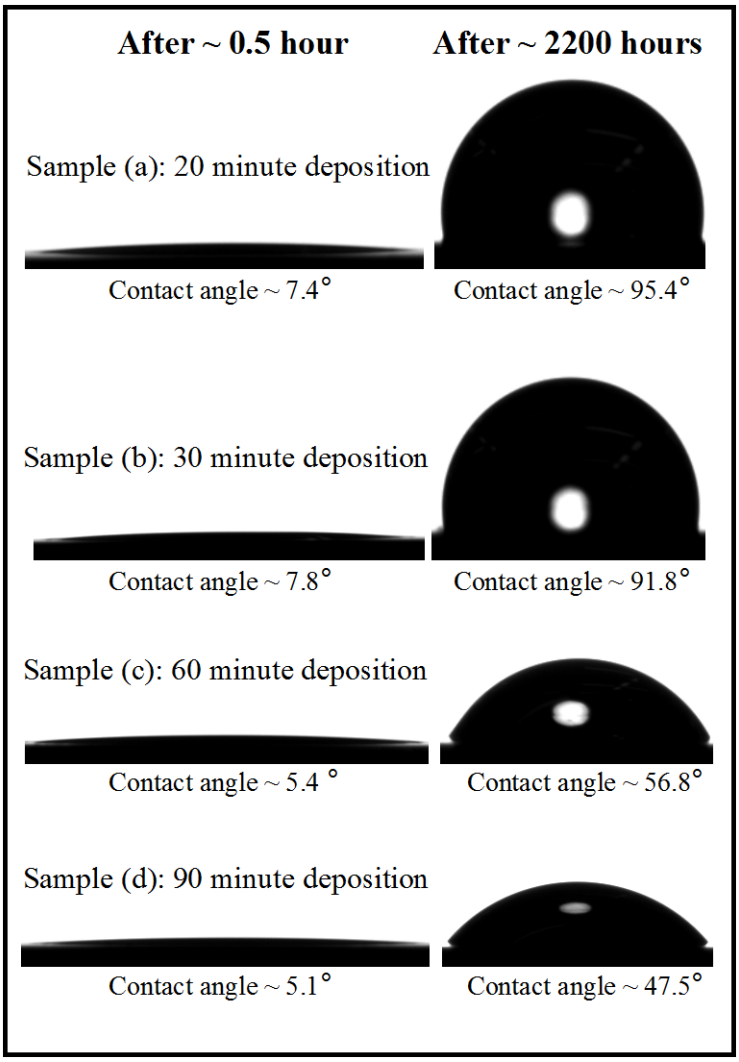

Fig: 3.1: Water droplets on fresh prepared and aged Ni nanorod arrays with different height. First column was taken after the samples were removed from the vacuum chamber about 30 minutes, and second column was taken after about three months.

For each sample, the measurements of water contact angles were taken in a sequence of aging time in air spanning a period of three months. The first measurement was taken immediately after the samples were removed from the vacuum chamber, which has about 30 minutes aging time. Last measurement was taken after about three months aging time. For each measurement, a water droplet was placed in a unique location. Also an experiment was performed where we dropped a droplet on a new place or on a previous place after it completely dry; this gave the same result shown in Figure 3.2.

The nickel nanorod arrays of all samples were completely wetted right after the deposition. The measured contact angles for all samples are in the range of 5 and 8^{o}. Since they are just made from pure metal inside the vacuum chamber, the samples were almost clean and free of contamination. Therefore, the nanorod stays in the superhydrophillic region. With increasing aging time, the observed water contact angles increases for all samples. However after around three months, the water contact angle increases in two different groups. Some samples have large increase of water contact angles and change from hydrophilic to hydrophobic; and the rest of the samples have small increase of water contact angles and stay in the hydrophilic region. In the both sets of samples, the water contact angles of samples with 10, 20, 30, 45 and 50 minutes deposition time, and the addition sample at second set of samples with 55 minutes deposition time, water contact angles increase more than or around 90°during 90 days; Whereas the samples with 60 and 90 minutes deposition time in both sets of samples water contact angles are not more than 60° over the same period of aging time in air. The images of the water sessile drops shown in Fig. 3.1 are an example of samples from first group that changed from hydrophilic to hydrophobic, and samples from second group that stayed in hydrophilic range. There is no difference of the measured contact angles at different places on the same sample surface, nor the sample places with previous measurement, as can be seen in Fig. 3.2.

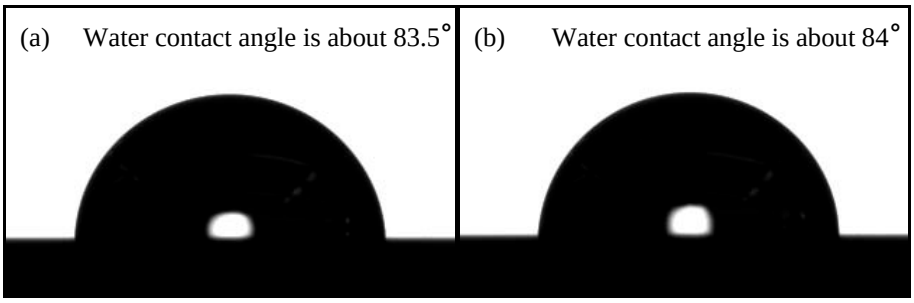

Fig. 3.2: The water droplets after six weeks in different places on the same sample. (a) is the droplet on a new place and (b) is the droplet on a place with previously deposited water droplet. The contact angles are the same for (a) and (b).

The changing of water contact angles for samples with aging time in air: for the first set of samples is shown in Fig. 3.3, and for the second set of samples is shown in Fig.3.4. Fig. 3.3 shows a gap between the sample with 50 min deposition time and the sample with 60 min deposition time due to the extremely large different in their nanorods height; however the heights of nanorods in the second set of samples are slightly close to each other. The structure parameters of nanorods will be discussed later in chapter 4.

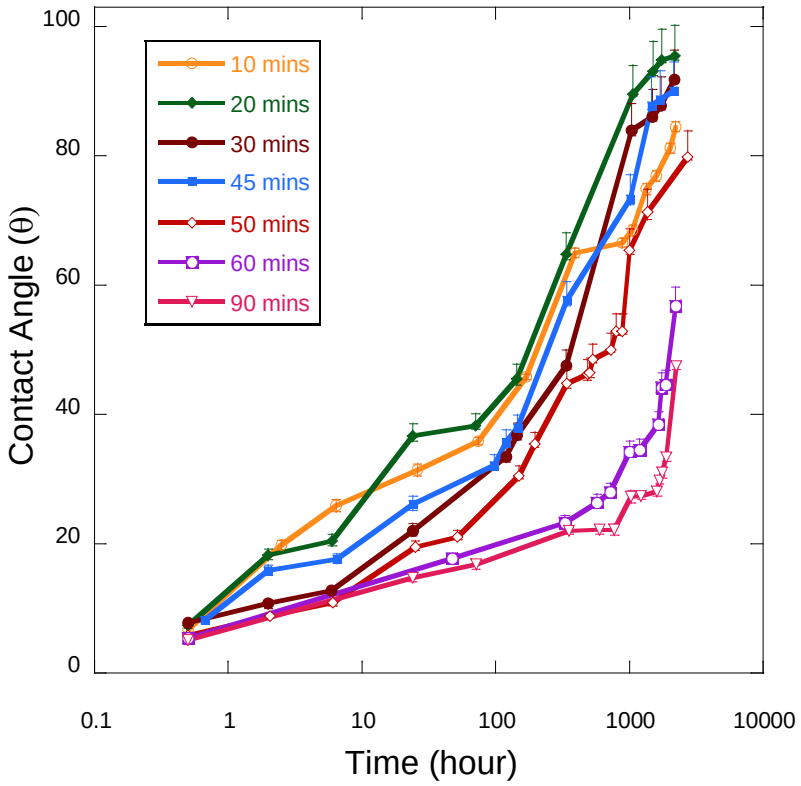

Fig. 3.3: Water contact angles of first set of samples change with aging time in air.

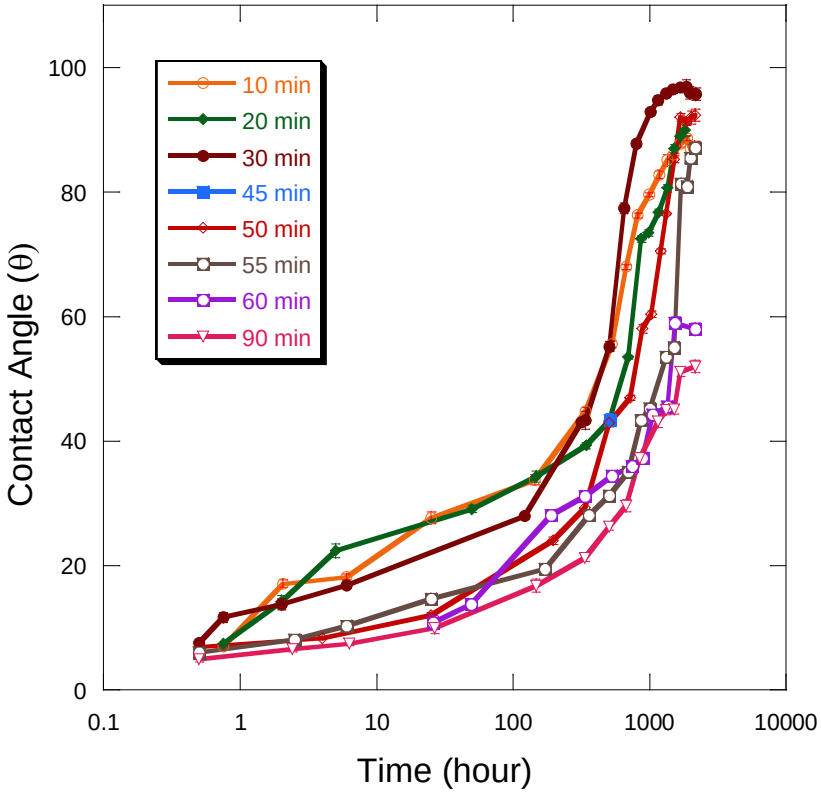

Fig. 3.4: Water contact angles of second set of samples change with aging time in air.

Chapter 4: Morphology

From the SEM images, we can observe how the morphology of the nickel nanorods changes for each sample. Cross-section images show an increase in the height of nanorods that corresponds with the increase of deposition time. Therefore, the nanorods of samples with 20 minute deposition have higher nanorods than those of samples with 10 minute deposition. This trend can be observed for longer deposition times as well (e.g.: 30, 45, 50 min). A nanotip was observed to appear on the top of the nanorod; however these nanotips are more clearly seen on the samples with deposition times from 45 minutes and up.

The top view of the SEM images allows the diameter of the nanorods and the separation between them to be measured. The diameter and the separation also increase with an increase in the deposition time. The ratio of the diameter to the separation is very similar for all the samples. Table 4.1 and 4.2 give a summary of all the data. The SEM images of the first set of samples are shown in Fig. 4.8, and the images for the second set of samples are shown in Fig. 4.9.

The roughness ratio was calculated for each sample by using equation (4) and (5), and based on the structural parameters of the nanorods of both sets given in Table 4.1 and Table 4.2. Figure 4.1 and Figure 4.2 show the relationship between roughness ratio and water contact angle for first and second sets of samples, respectively. Figure 4.3 shows the roughness ratio corresponding to the height of the nanorods for first set of samples, and Figure 4.4 shows the roughness ratio corresponding to the height of the nanorods for second set of samples.

Table 4.1: The structural parameters obtained from the SEM images of the nickel nanorods for the first set of samples. Also included are the roughness ratio results.

Samples (Deposition time)	Diameter D (nm)	Separation L (nm)	Height H (nm)	roughness ratio (r)	D/L
10 min	15.3 ± 3	23 ± 6.6	52 ± 3.5	5.7	0.7
20 min	27.2 ± 7.6	36.8 ± 12.4	135.8 ± 4.6	9.6	0.7
30 min	31.3 ± 10	44.4 ± 12.4	175.1 ± 8.7	9.7	o.7
45 min	36 ± 14.2	45 ± 13.9	222.5 ± 8.5	12.6	0.8
50 min	55.4 ± 22.5	72.5 ± 27.3	353.7 ± 13.8	12	0.8
60 min	66.6 ± 23	109.3 ± 50.7	566.8 ± 21.8	10.5	0.7
90 min	85 ± 49.2	131 ± 60	613.9 ± 31	10	0.8

Table 4.2: The structural parameters obtained from the SEM images of the nickel nanorods from the second set of samples. Also included are the roughness ratio results.

Samples (Deposition time)	Diameter D (nm)	Separation L (nm)	Height H (nm)	roughness ratio (r)	D/L
10 min	14 ± 5	22 ± 6.6	43.5 ± 4	5	0.6
20 min	21 ± 6.6	26.2 ± 7	65.4 ± 5.8	7.2	0.8
30 min	29.5 ± 12	41± 12	118 ± 8.5	7.4	o.7
45 min	38.6 ± 16.2	51 ± 20	175.4 ± 10	8.5	0.7
50 min	43.2 ± 14.4	53 ± 19.4	176.4 ± 2.8	8.7	0.8
55 min	43.7 ± 15.6	61 ± 23.5	179.7 ± 3	7	0.7
60 min	47 ± 14.4	67.6 ± 18.2	196.3 ± 2.8	6.7	0.7
90 min	54 ± 21	89.8 ± 42.4	283.3 ± 1.8	6.5	0.6

The relationship between the water contact angles and roughness ratio *r* was studied according to Wenzel model in this thesis. Fig. 4.1 and Fig. 4.2 show these relationships of first and second sets of samples with the roughness ratio r calculated from the equations (4) and (5) developed in Chap. 2. However there is no correlation between the water contact angles and the roughness ratio r. Wenzel model didn't fit or helped in explaining our results. The reason is mainly due to samples are too rough. In this case we studied the relationship between the water contact angles and nanorods height as shown in figure from 4.3 to 4.7.

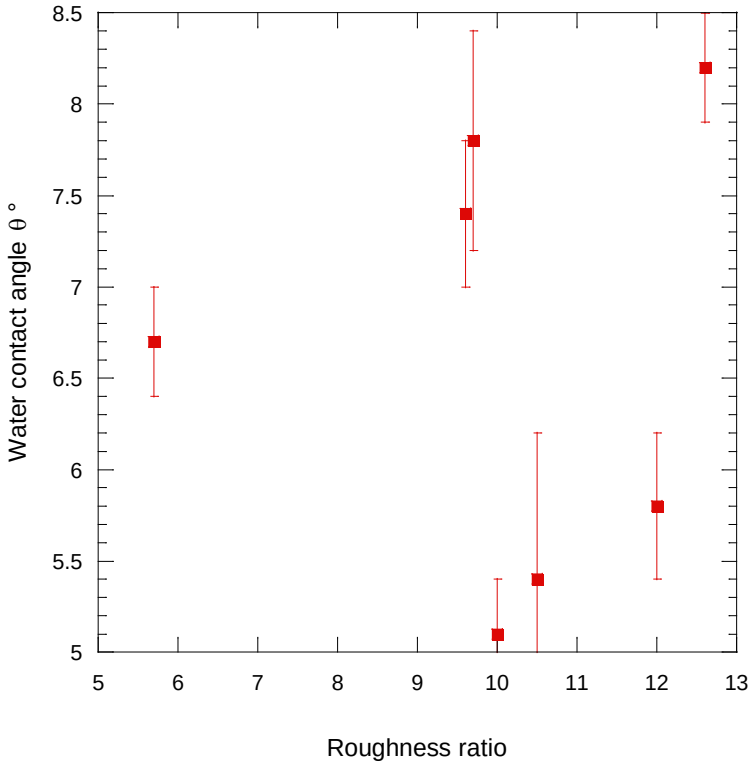

Fig. 4.1: The roughness ratio versus water contact angles for the first set of samples.

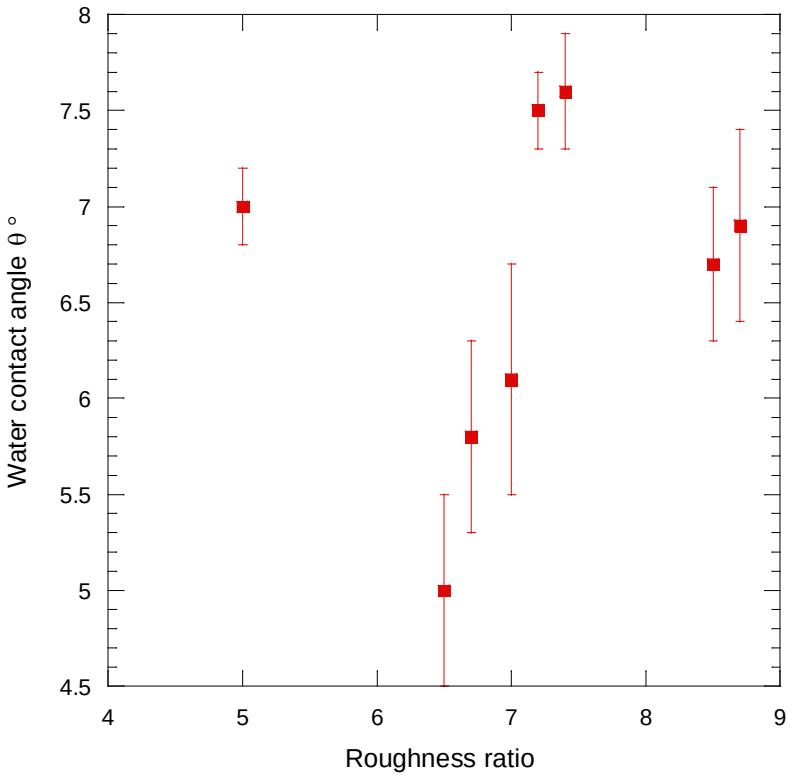

Fig. 4.2: The roughness ratio versus water contact angles for the second set of samples.

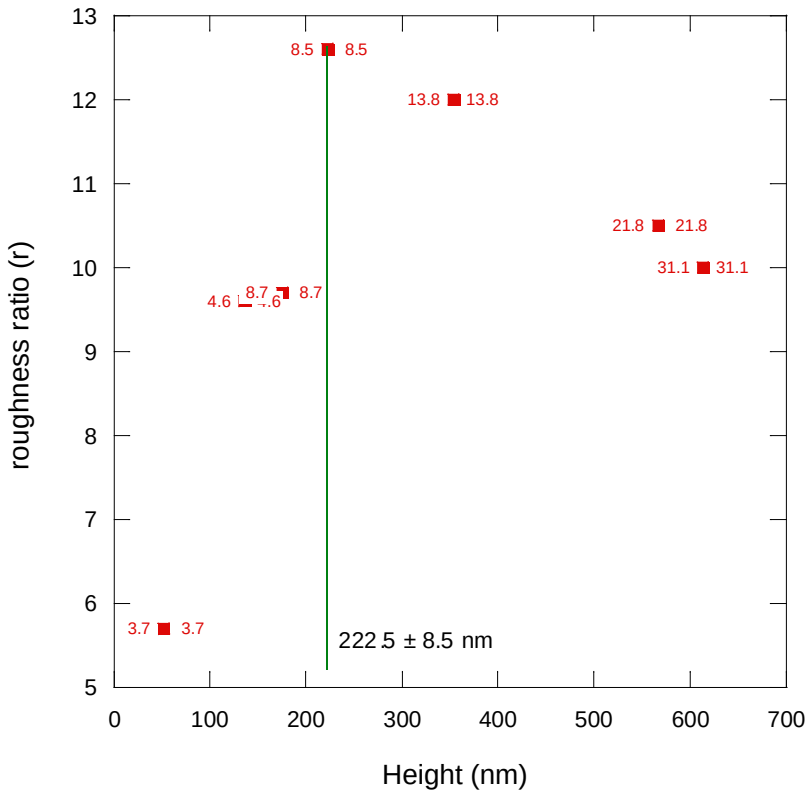

Fig. 4.3: The roughness ratio versus the height of the nanorods for the first set of samples.

In Fig. 4.3 the roughness ratio increases with the height of the nanorods until the height reaches 222.5 ± 8.5 nm; this is the height of the sample that was deposited for 45 minutes in first sample set. After this value, the roughness begins to decrease. The sample with a 50 minute deposition time exhibits a decrease in the roughness even with an increase in height.

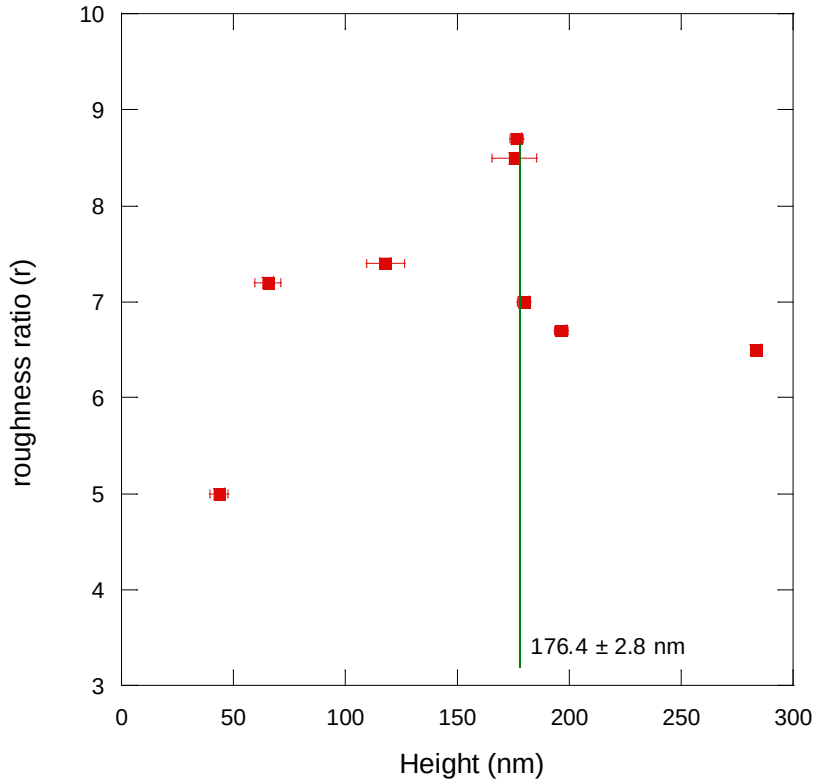

Fig. 4.4: The roughness ratio versus the height of the nanorods for the second set of samples.

In Fig. 4.4 the roughness ratio increases with the height of the nanorods until the height reaches 176.4 ± 2.8 nm in second set of samples. This height is related to the sample that was deposited for 50 minutes. The roughness of sample with the next time deposition which is 55 minute begins to decrease after that with an increase in height.

In Fig 4.5 and Fig 4.6, the relationship between the height of the nanorods and the water contact angle are displayed for the same aging time lengths in air for the first and second set of samples, respectively. However, the aging times are displayed after approximately 30 min, fifteen days, forty three days and 90 days. At first, the measurements of all the samples were in the same range, but in the end, after approximately 90 days, when the samples reached equilibrium, the water contact angle increased slightly with the height of the nanorods, then decreased. The increase in water contact angles for all samples with aging time in air changed with a large value during the first month of taking the measurements, then start changing with small values.

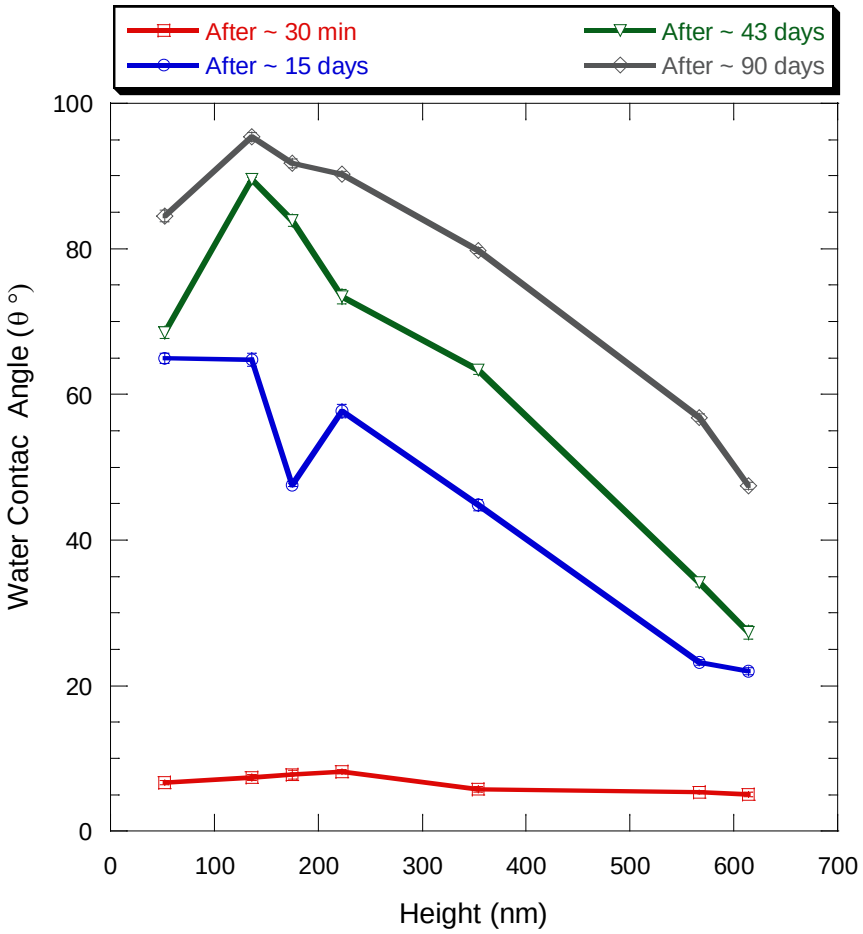

Fig. 4.5: The relationship between the height of the nanorods for the first set of samples to the water contact angles that were taken at similar aging times in air.

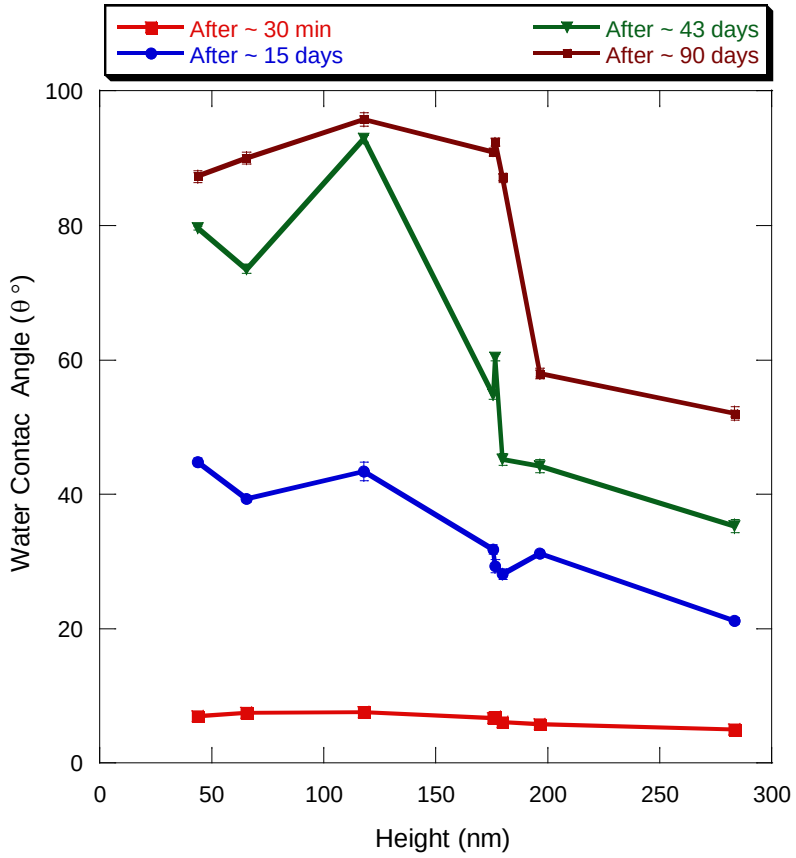

Fig. 4.6: The relationship between the height of the nanorods for the second set of samples to the water contact angles that were taken at similar aging times in air.

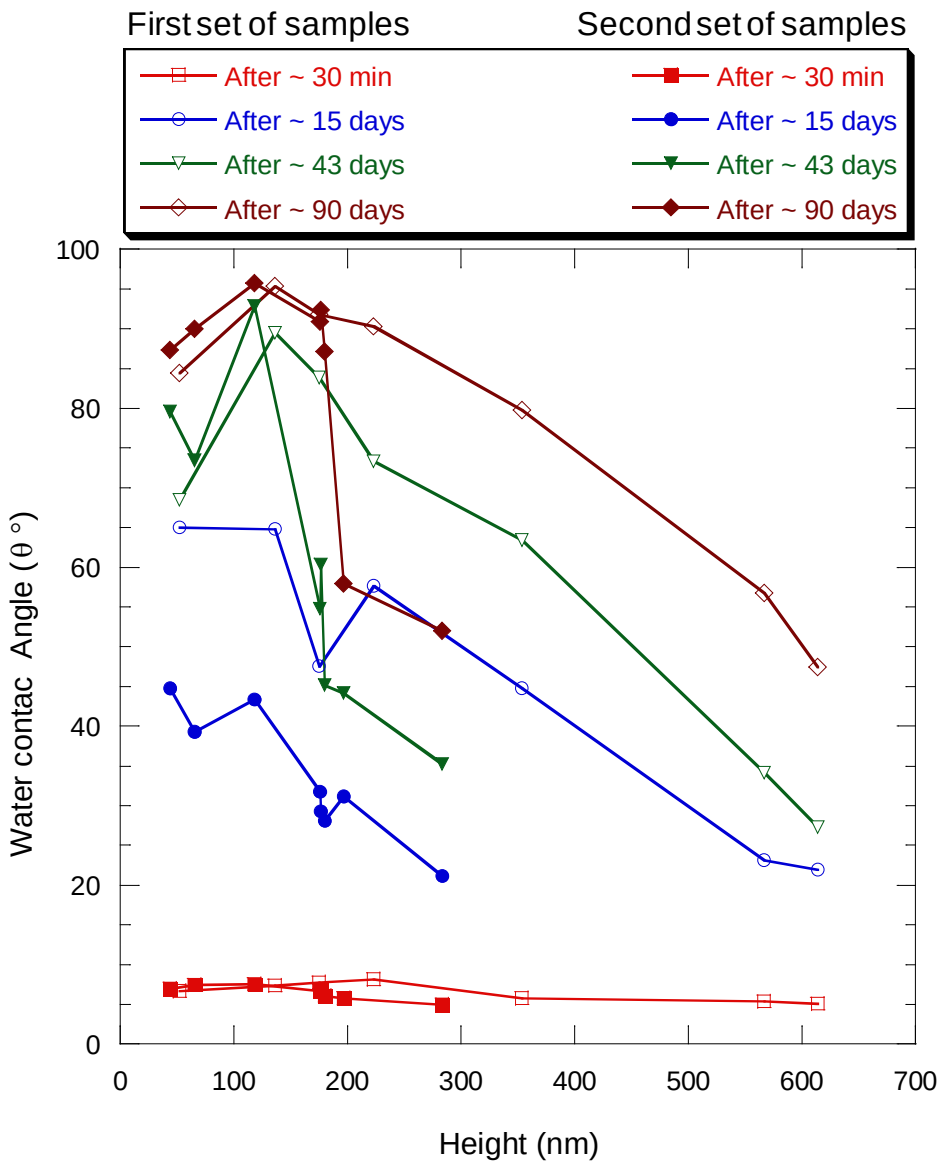

Fig. 4.7: The relationship between the height of the nanorods for both sets of samples to the water contact angles that were taken at similar aging times in air.

SEM Images of the First Set of Samples

Top View Cross Section

Sample with 10 min deposition

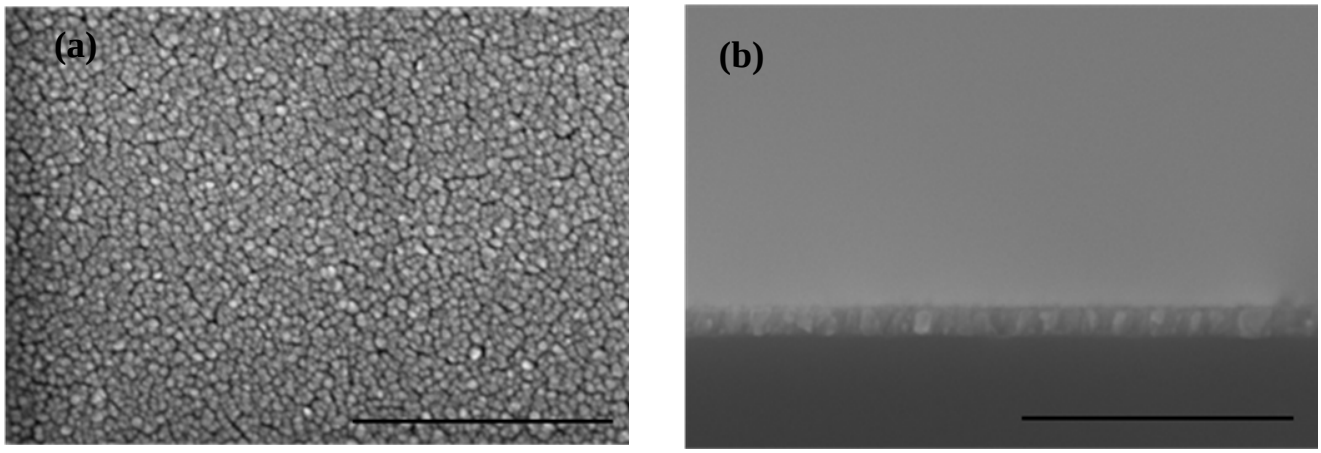

Diameter of Rods ~ 15.3 ± 3.1 nm

Height of Rods ~ 135.8 ± 4.6 nm

Sample with 20 min deposition

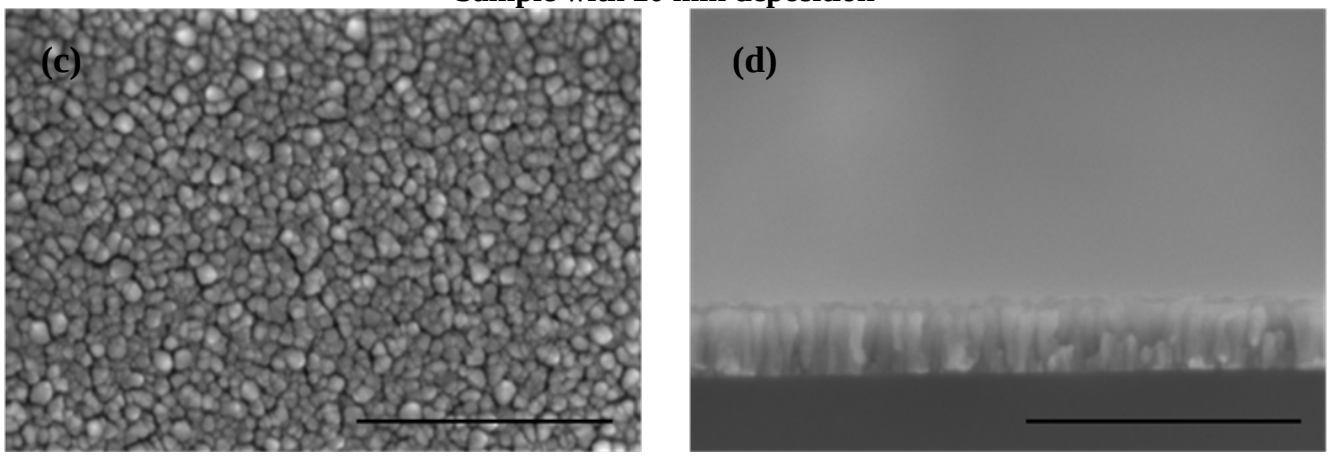

Diameter of Rods ~ 27.2 ± 7.6 nm

Height of Rods ~ 135.8 ± 4.6 nm

Fig. 4.8: Scanning electron microscopy (SEM) images of the first set of samples of nickel nanorods of (a), (b) sample with 10 min deposition of top view and cross section, respectively, (c) and (d) sample with 20 min deposition of top view and cross section, respectively. The scale bars of the SEM micrograph are 500 nm.

Top View Cross Section

Sample with 30 min deposition

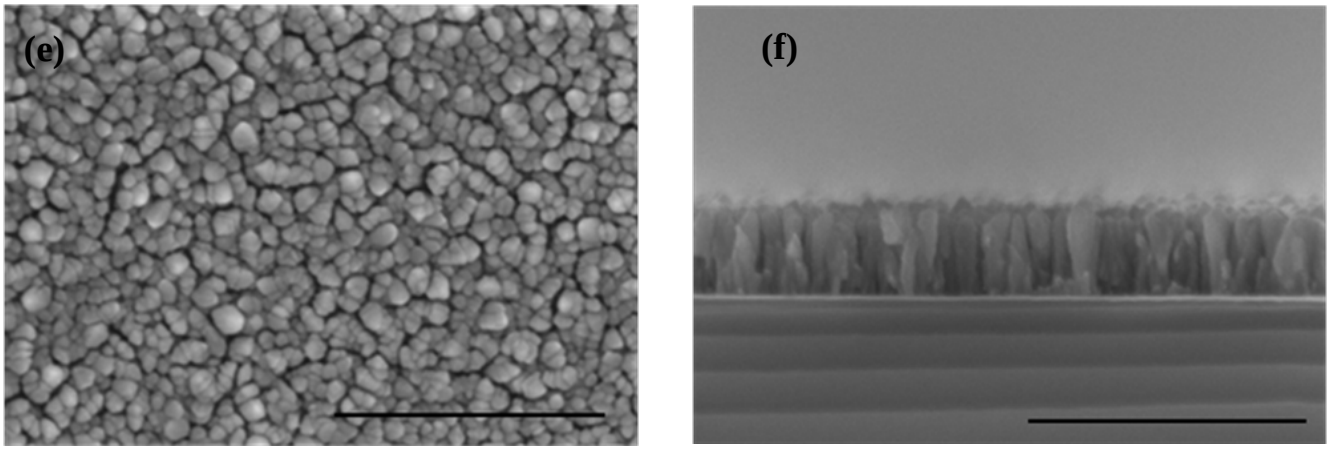

Diameter of Rods ~ 31.3 ± 10.1 nm Height of Rods ~ 175.1 ± 8.7 nm

Sample with 45 min deposition

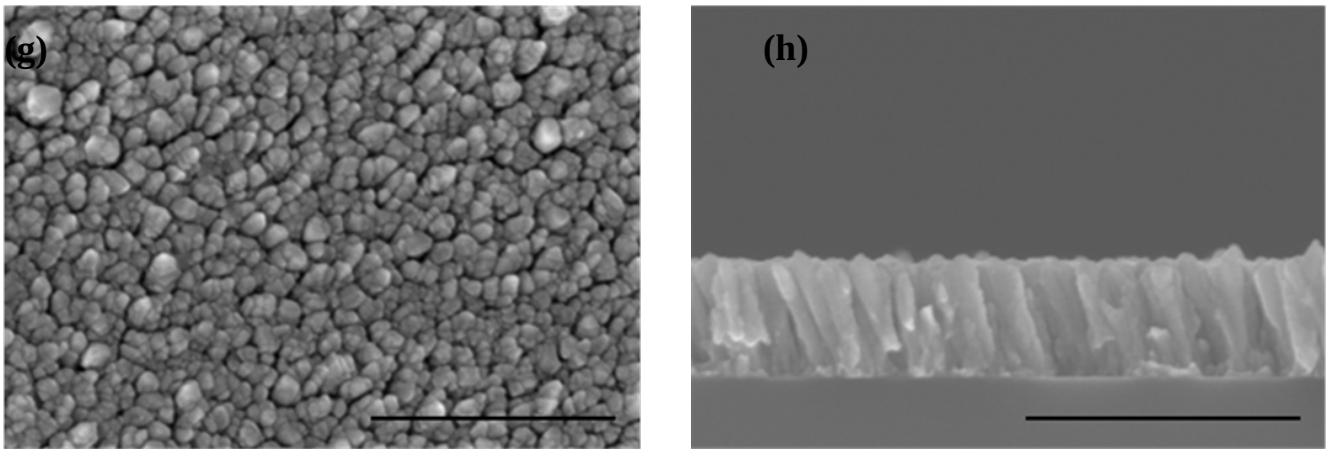

Diameter of Rods ~ 36.1 ± 14.2 nm Height of Rods ~ 222.5 ± 8.5 nm

Fig. 4.8: Scanning electron microscopy (SEM) images of the first set of samples of nickel nanorods of (e), (f) sample with 30 min deposition of top view and cross section, respectively, (g) and (h) sample with 45 min deposition of top view and cross section, respectively. The scale bars of the SEM micrograph are 500 nm.

Top View Cross Section

Sample with 50 min deposition

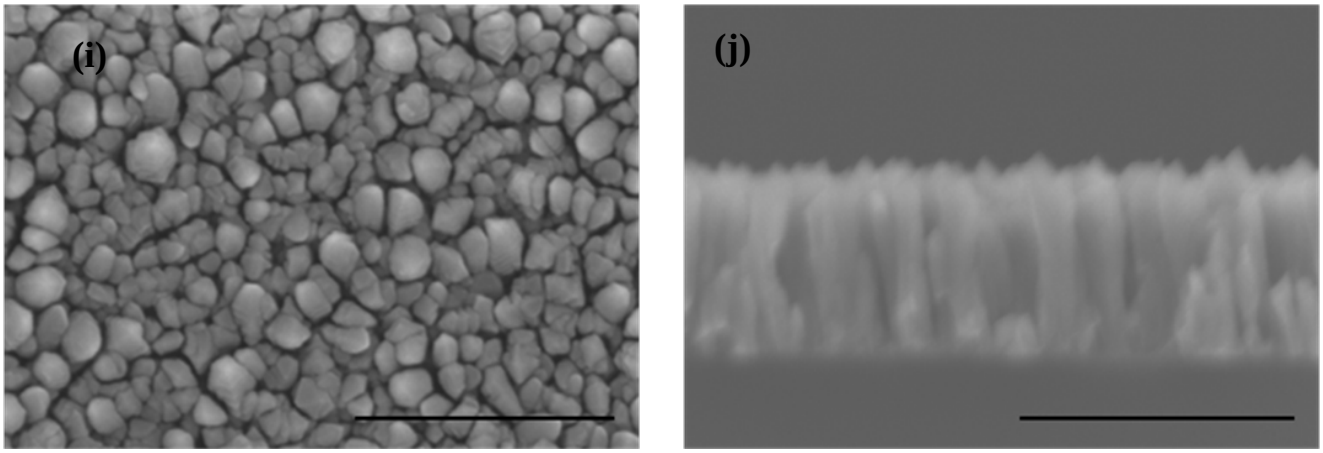

Diameter of Rods ~ 55.4 ± 22.5 nm Height of Rods ~ 353.7 ± 13.8 nm

Sample with 60 min deposition

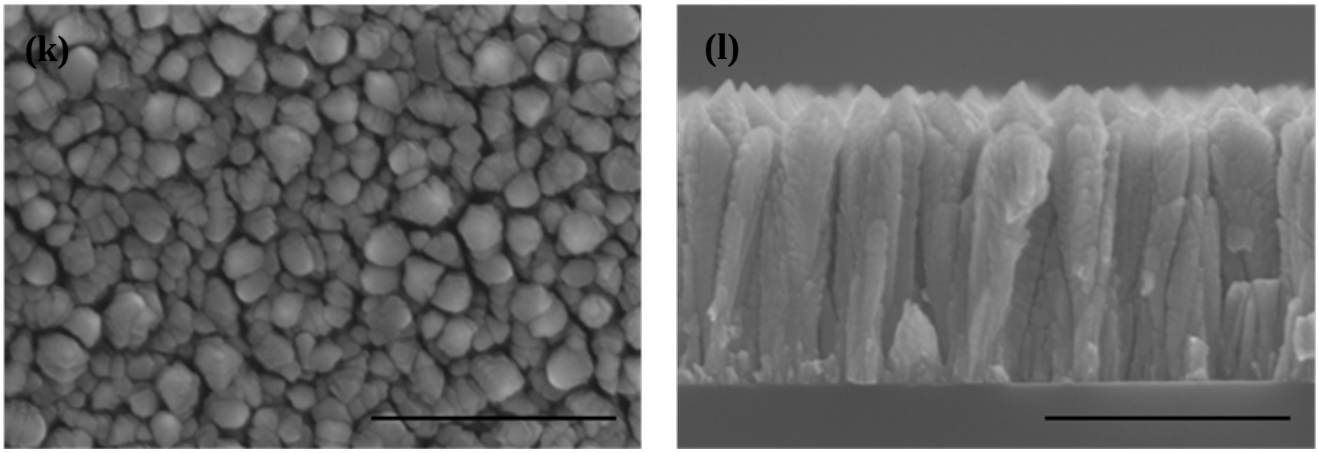

Diameter of Rods ~ 66.6 ± 23 nm Height of Rods ~ 566.8 ± 21.8 nm

Fig. 4.8: Scanning electron microscopy (SEM) images of the first set of samples of nickel nanorods of (i), (j) sample with 50 min deposition of top view and cross section, respectively, (k) and (l) sample with 60 min deposition of top view and cross section, respectively. The scale bars of the SEM micrograph are 500 nm.

Top View Cross Section

Sample with 90 min deposition

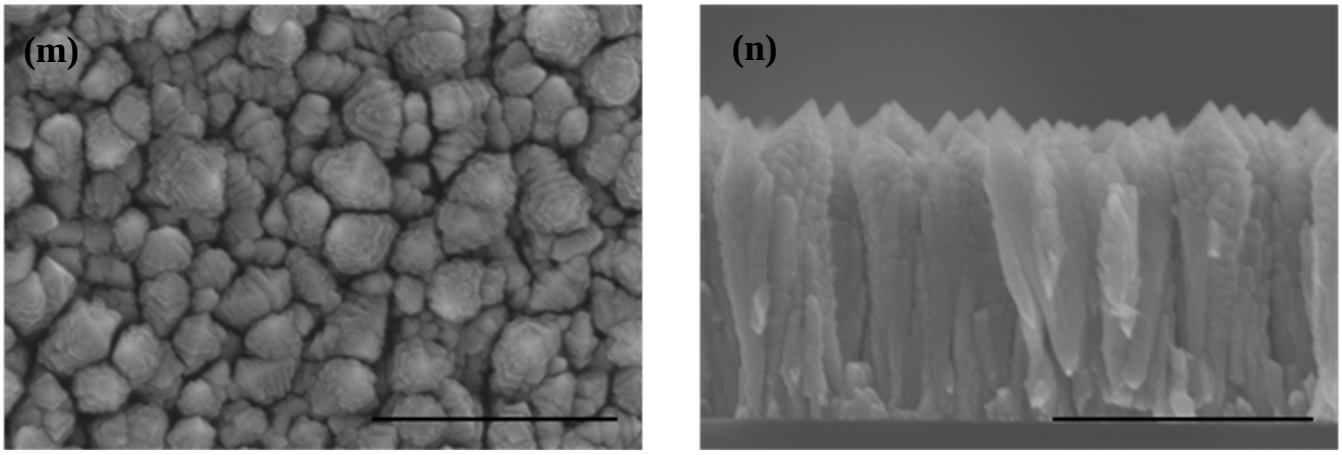

Diameter of Rods ~ 85.1 ± 49.2 nm Height of Rods ~ 613.9 ± 31.1 nm

Fig. 4.8: Scanning electron microscopy (SEM) images of the first set of samples of nickel nanorods of (m), (n) sample with 90 min deposition of top view and cross section, respectively. The scale bars of the SEM micrograph are 500 nm.

SEM Images of the Second Set of Samples

Top View Cross Section

Sample with 10 min deposition

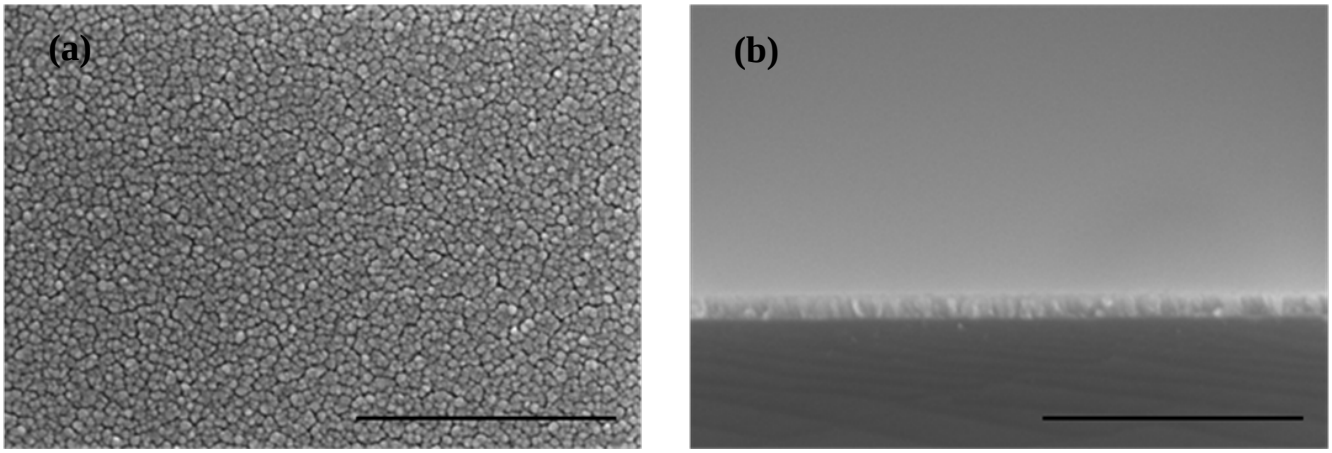

Diameter of Rods ~ 14 ± 5 nm

Height of Rods ~ 43.5 ± 4 nm

Sample with 20 min deposition

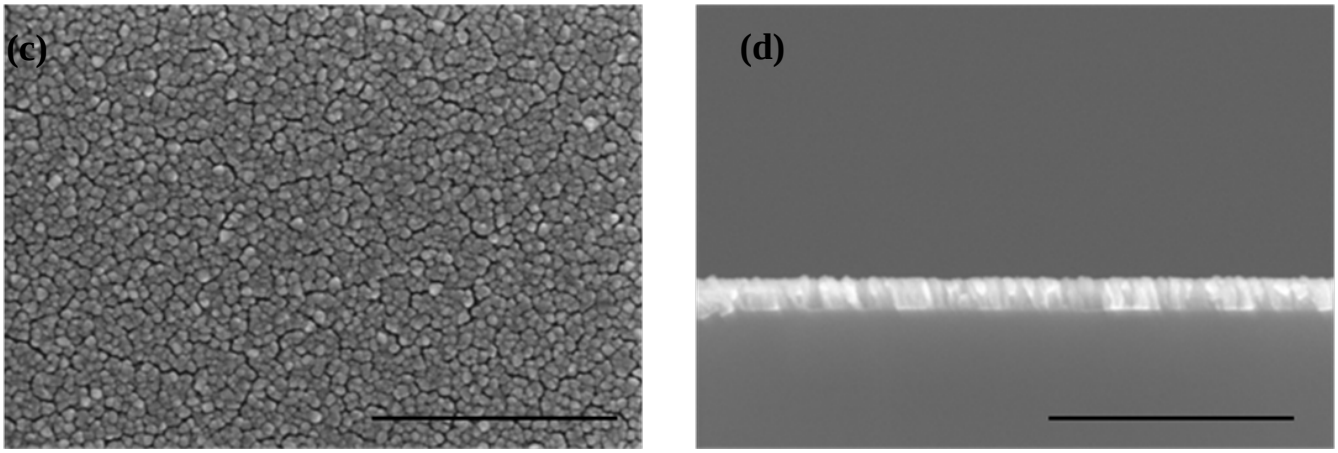

Diameter of Rods ~ 21 ± 6.6 nm

Height of Rods ~ 65.4 ± 5.8 nm

Fig. 4.9: Scanning electron microscopy (SEM) images of the second set of samples of nickel nanorods of (a), (b) sample with 10 min deposition of top view and cross section, respectively, (c) and (d) sample with 20 min deposition of top view and cross section, respectively. The scale bars of the SEM micrograph are 500 nm.

Top View Cross Section

Sample with 30 min deposition

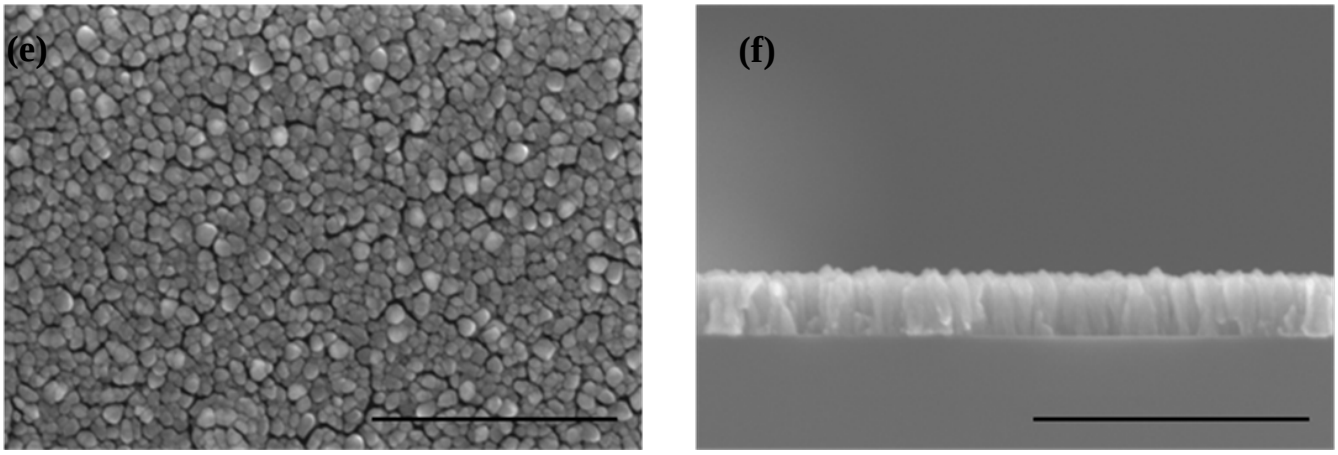

Diameter of Rods ~ 29.5 ± 12 nm

Height of Rods ~ 118 ± 8.5 nm

Sample with 45 min deposition

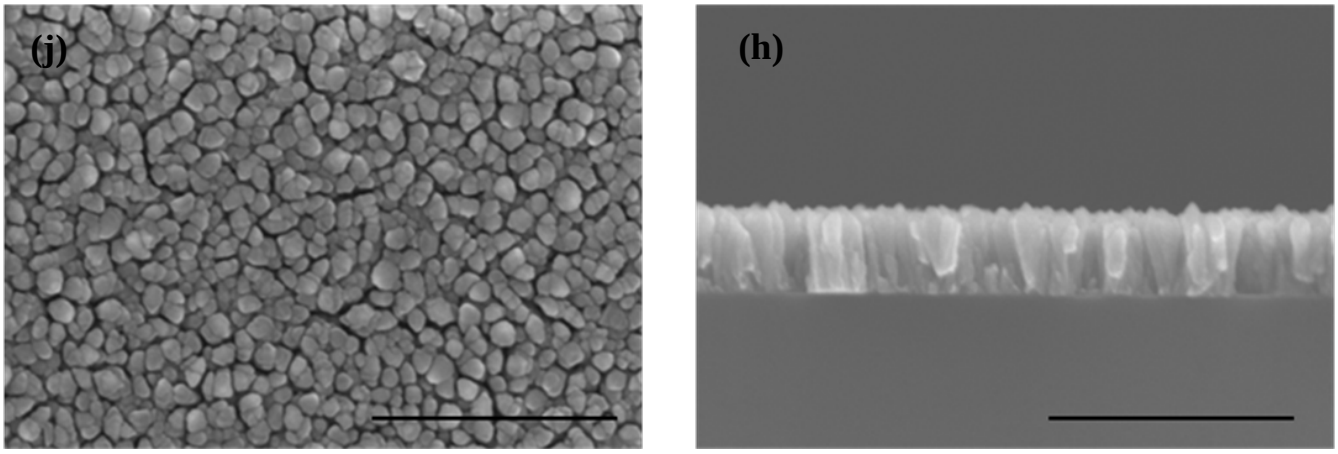

Diameter of Rods ~ 38.6 ± 16.2 nm

Height of Rods ~ 175.4 ± 10 nm

Fig. 4.9: Scanning electron microscopy (SEM) images of the second set of samples of nickel nanorods of (e), (f) sample with 30 min deposition of top view and cross section, respectively, (j) and (h) sample with 45 min deposition of top view and cross section, respectively. The scale bars of the SEM micrograph are 500 nm.

Top View Cross Section

Sample with 50 min deposition

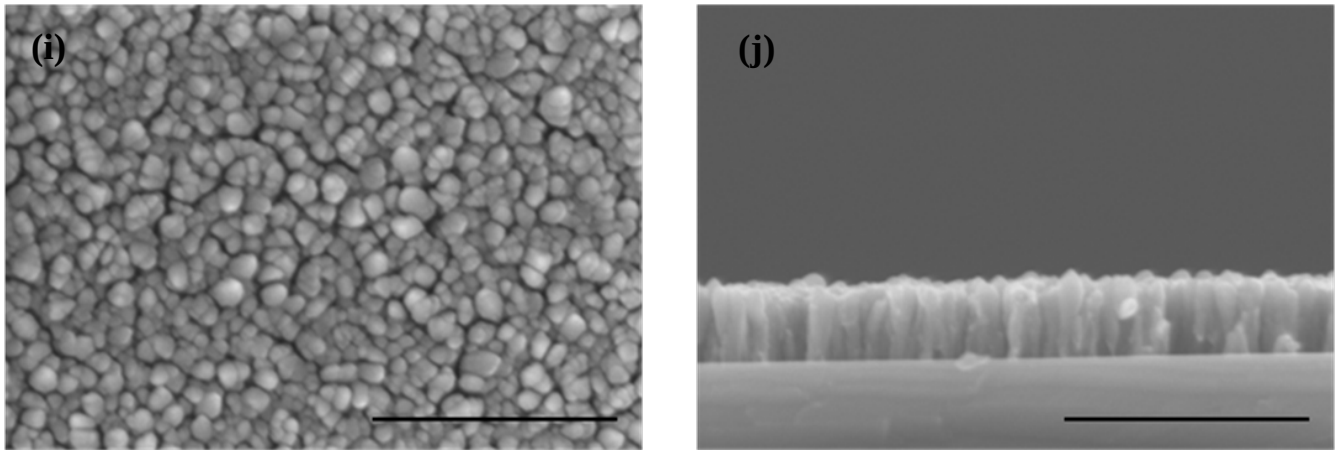

Diameter of Rods ~ 43.2 ± 14.4 nm Height of Rods ~ 176.4 ± 2.8 nm

Sample with 55 min deposition

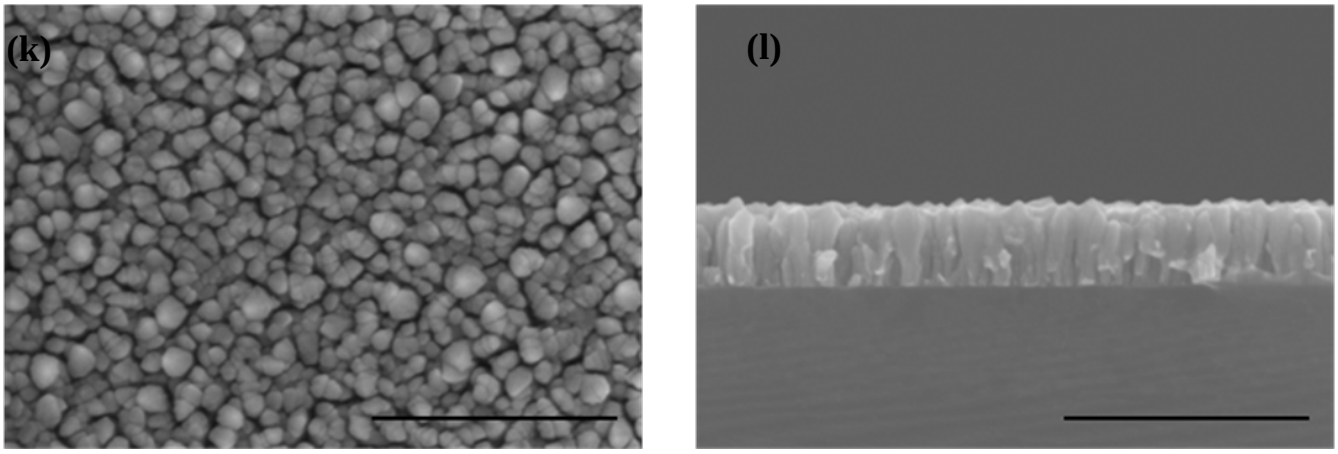

Diameter of Rods ~ 43.7 ± 15.6 nm Height of Rods ~ 179.7 ± 3 nm

Fig. 4.9: Scanning electron microscopy (SEM) images of the second set of samples of nickel nanorods of (i), (j) sample with 50 min deposition of top view and cross section, respectively, (k) and (l) sample with 55 min deposition of top view and cross section, respectively. The scale bars of the SEM micrograph are 500 nm.

Top View Cross Section

Sample with 60 min deposition

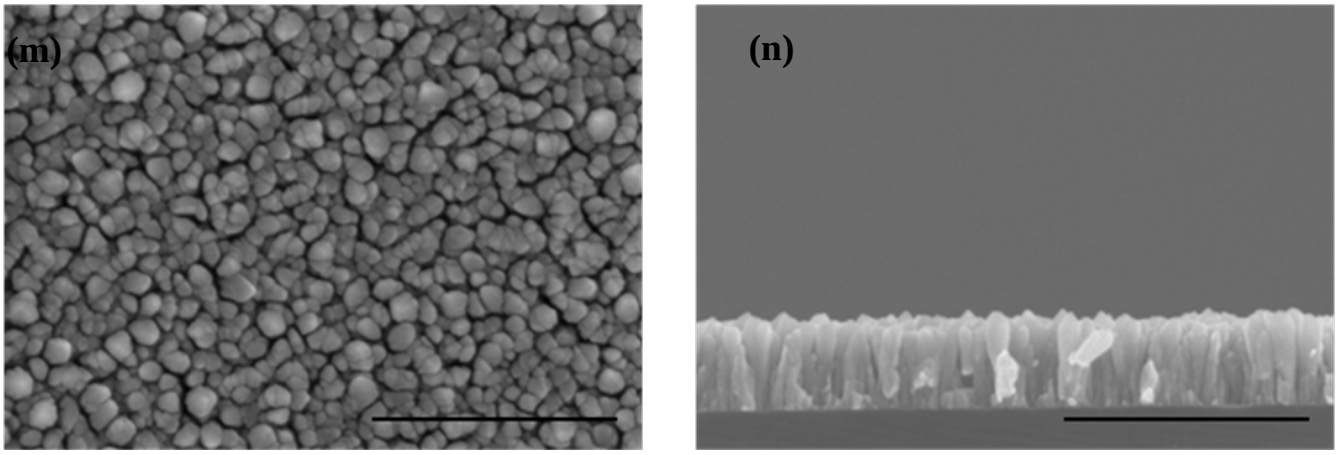

Diameter of Rods ~ 47 ± 14.4 nm Height of Rods ~ 196.3 ± 2.8 nm

Sample with 90 min deposition

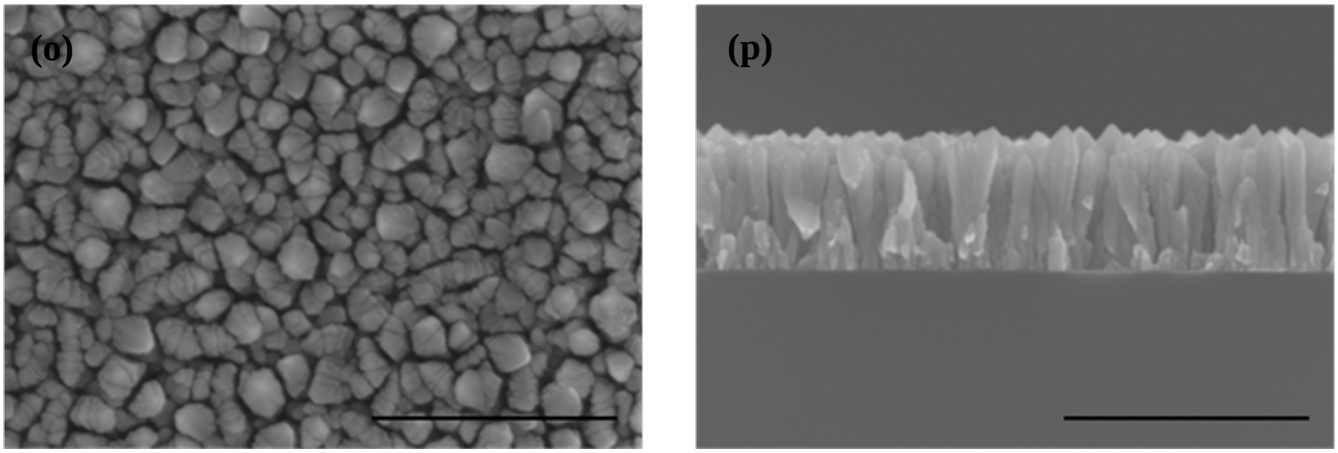

Diameter of Rods ~ 54 ± 21 nm Height of Rods ~ 283.3 ± 1.8 nm

Fig. 4.9: Scanning electron microscopy (SEM) images of the second set of samples of nickel nanorods of (m), (n) sample with 60 min deposition of top view and cross section, respectively, (o) and (p) sample with 90 min deposition of top view and cross section, respectively. The scale bars of the SEM micrograph.

Chapter 5: Contamination

Contamination may be responsible to the aging effect we observed in the contact angle experiments. X-ray photoelectron spectroscopy (XPS) was used to monitor chemical changes on the sample surface over aging time in air. The first analysis was done immediately when the samples just removed from the chamber where they made, and that was after around 30 minutes exposing to air. Subsequent measurements were performed about one month and two months later on the same sample. XPS was performed on one sample from each of the rate groups: the first group, the water contact angles changed from hydrophilic to hydrophobic within the period of observation aging time. The second group, the water contact angles increased over the same period of aging time but stayed in the hydrophilic range. The samples chosen were a 20 minutes deposition with 65.4 ± 5.8 nm height, and 60 minutes deposition with 196.3 ± 2.8 nm height. The first, second and third analysis of both samples are shown in figures (5.1), (5.2) and (5.3) respectively.

XPS spectra of nickel were analyzed. The binding energies were corrected for all samples and calibrated regarding the charging effect by referencing the C 1s to neutral carbon peak at 285 eV. The survey-scan XPS spectra showed different peaks. Different peaks related to the binding energies of nickel (Ni2p, Ni3s and Ni3p), oxygen (O1s), carbon (C1s) and Auger peaks. However the XPS analysis of same samples at one-month old and two-months old showed a smaller amount of one more element, Silicon (Si 2p), which was the substrate of nanorods. XPS survey spectra are shown in Figures (5.1.a), (5.2.a) and (5.3.a).

XPS high resolution spectra were recorded for nickel (Ni2p), oxygen (O1s) and carbon (C1s). Figures (5.1.b), (5.2.b) and (5.3.b) illustrate the core-level spectra for the Ni 2p. Ni 2p exhibits doublet peaks due to the spin-orbit coupling in 2p orbital. For both samples over aging time in air, the two peaks are centered at 852.5eV and 869.9 eV, corresponding to Ni 2p3/2 and Ni 2p1/2. The separation between the two peaks is 17.4 eV, which agrees with standard values.[12] There are two peaks in addition to the two major peaks in the spectra, which are caused by the chemical shift due to oxidized Ni. These two peaks are attributed to two different oxidation states of Ni at 855.6 eV and

860.9 eV.[13] Figures (5.1.c), (5.2.c) and (5.3.c) showed the XPS high resolution spectra for oxygen (O1s) binding energies. From these figures, it can be seen that for both samples over aging time in air, the spectrum displays two O1s peaks at 529.7 eV and 531.5 eV. These two values of binding energies could be related to different states of oxidation on the Ni nanorod surface. The peak centered at 529.7 eV is due to NiO, and it is the main stable oxide.[14] The other one centered at 531.5 eV is attributed to Ni_2O_3.[14, 15] Formation of this oxide indicates that the sample has both Ni^{2+} and Ni^{3+}.[16] The carbon (C1s) spectra of both samples taken at different aging time in air are shown in figures (5.1.d), (5.2.d) and (5.3.d). C1s is composed two peaks; one peak is the main peak that centered at 285 eV, while a small peak shows the chemical shift due to oxidation of carbon centered at about 288 eV.[17] All XPS data agree with standard values that are documented in the NIST database at their website, http://srdata.nist.gov/xps/.

Background subtraction is required in order to measure the peak area in the XPS spectra. The method used for the background removal in our XPS peaks is the "smart background subtraction" in the data process program provided by the manufacturer of the XPS system, which is based on the subtraction of Shirley background [18, 19] and linear background subtraction [20] to prevent the over subtraction. The over-subtraction of background can result a negative value of an XPS peak. The analysis of the XPS data was done based on the data in the survey spectra.

XPS spectra come from the ability of instrument to record the electrons that are ejected from the sample surface; not all the electrons that are removed out the samples are recorded by the instrument. The best way to compare XPS data is via the percentage atomic concentrations. The important point of using percentage atomic concentrations is to turn the intensities as percentages.[21] We calculated the percentage atomic concentrations via the formula: [22]

$$C_x = \frac{P_x / (ASF)_x}{\sum_i \frac{P_i}{(ASF)_i}} \qquad (6)$$

where Px is the peak area after background subtraction of element x, that are given in the program. (ASF)x is Atomic sensitive factors of element x and this is a standard values. Table 5.1 illustrates the percentage atomic concentrations of both samples.

Table 5.1: Percentage atomic concentrations of samples with 20 min and 60 min deposition over aging time in air.

Time / Elements	Sample with 20 min deposition			Sample with 60 min deposition		
	After ~ 30 min	After 36 days	After 60 days	After ~ 30 min	After 36 days	After 60 days
Ni2p	29.8	11	8.3	20.1	12.2	10
O1s	27.3	36.8	35.2	32.7	36.8	35.1
C1s	42.9	52.2	56.4	47.1	51	55

For the last measurement we took data in three different spots to verify the consistency of the XPS spectra. The results were very similar so we picked one to illustrate the behavior.

For the sample with a 20 min deposition time, the percentage atomic concentration of Ni2p decreased more than a half over 60 days. However, the O1s peak increased slightly after the initial measurement; The C1s peak also increased over aging time in air from 42.9% to 56.4%. For the sample with the 60 min deposition time, the percentage atomic concentration of Ni2p was decreased by a half over 60 days. The O1s behaved in the same manner as the 20 min deposition sample. For the C1s peak, it increased after 60 days from 47.1 % to 55%.

In case of increasing the O1s with aging time in air, the oxidation make the surface to be more hydrophilic.[8] In our studying, we observed increasing in water contact angles over aging time in air.

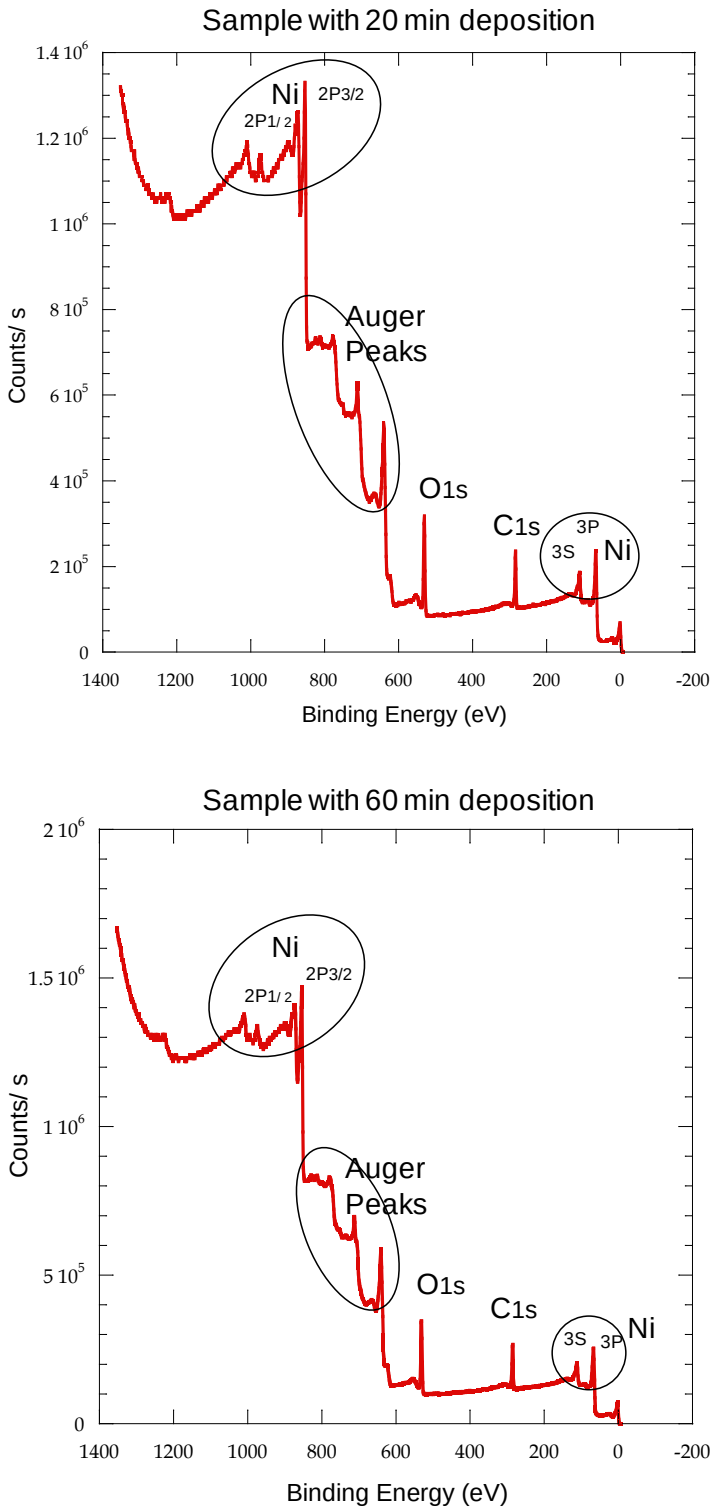

Fig 5.1 (a): XPS Survey spectra after ~ 30 min of samples with 20 min and 60 min deposition time.

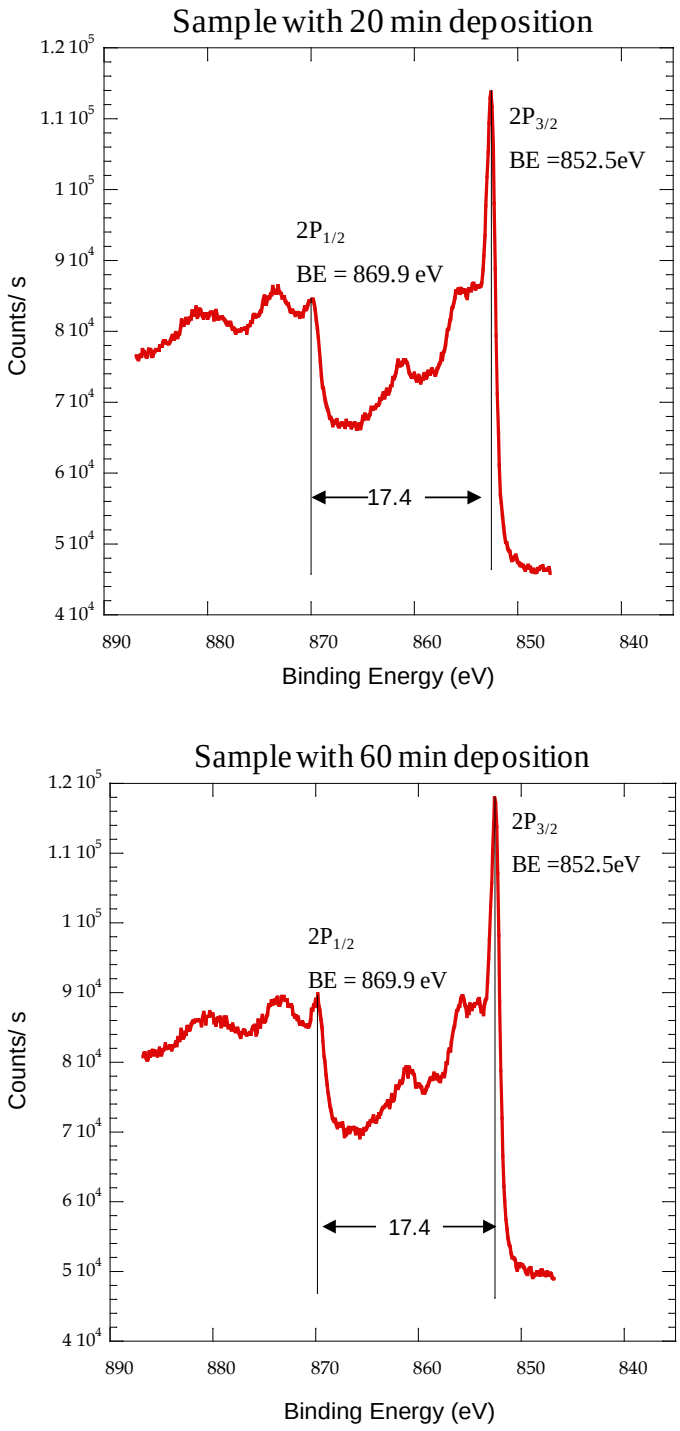

Fig 5.1 (b): XPS Core-level spectra of Ni2p after ~ 30 min of samples with a 20 min and 60 min deposition time.

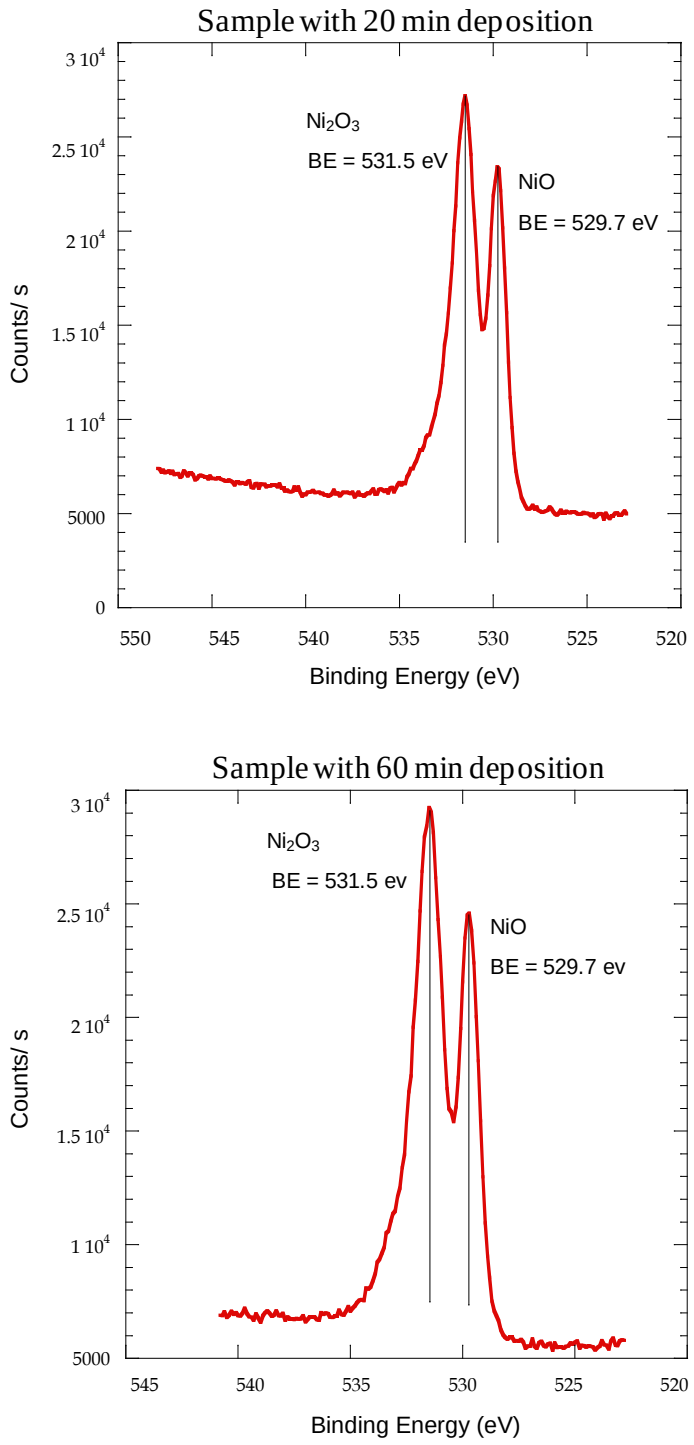

Fig 5.1 (c): XPS Core-level spectra of O1s after ~ 30 min of samples with a 20 min and 60 min deposition time.

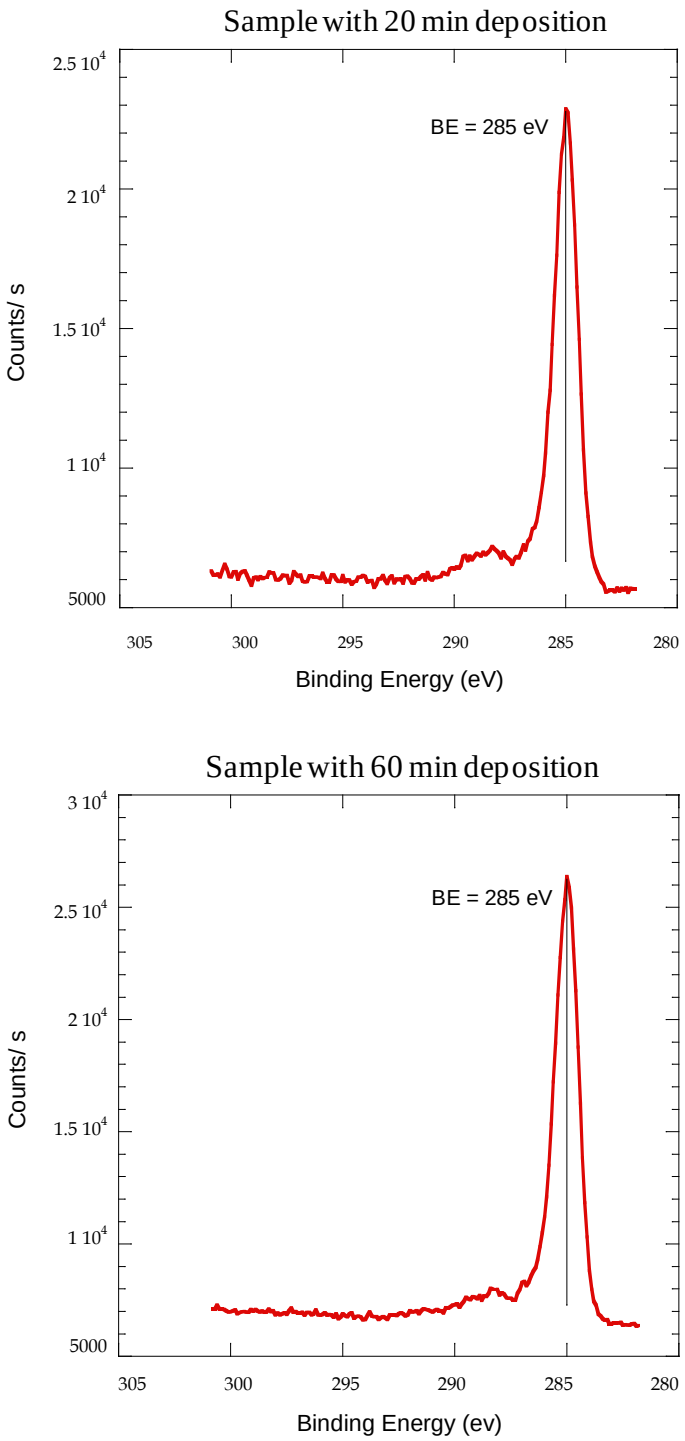

Fig 5.1 (d): XPS Core-level spectra of O1s after ~ 30 min of samples with a 20 min and 60 min deposition time.

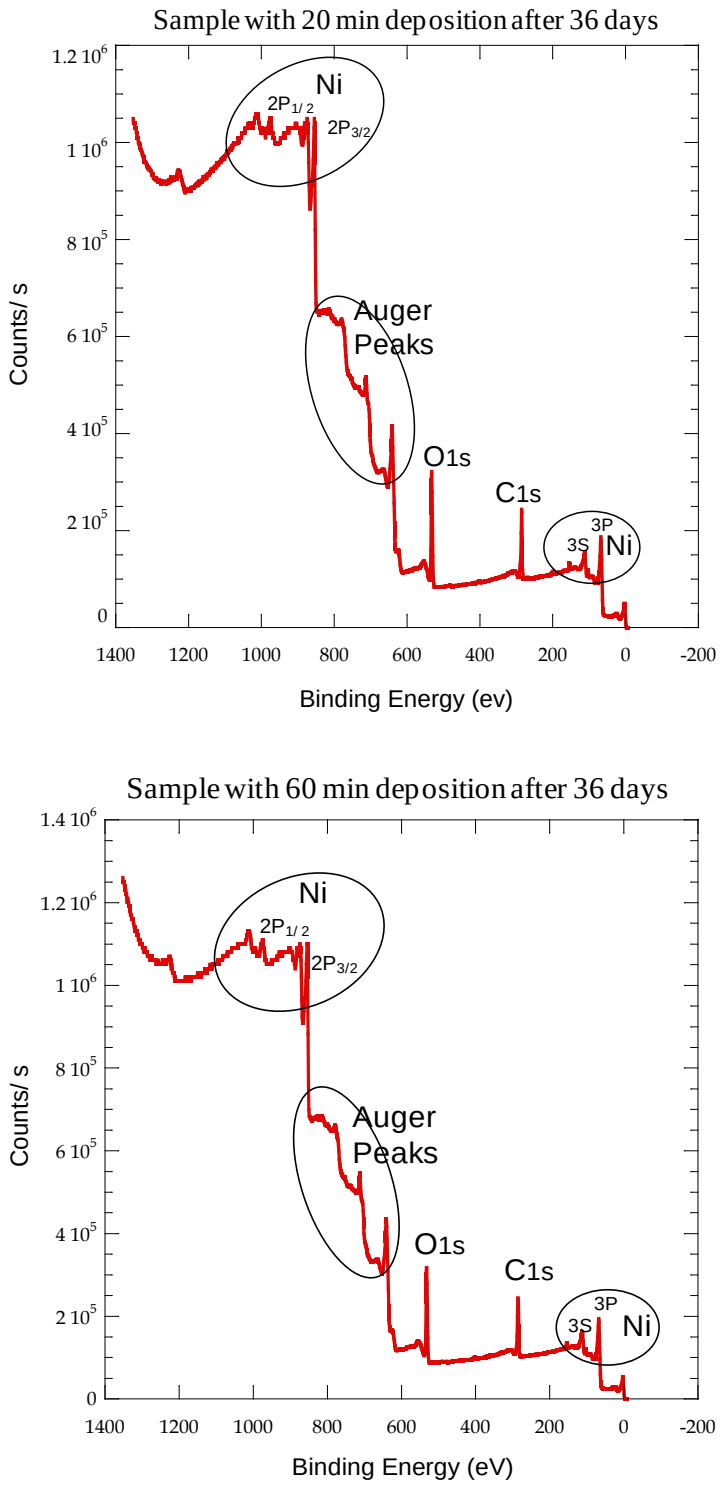

Fig 5.2 (a): XPS Survey spectrum after 36 days of samples with a 20 min and 60 min deposition time.

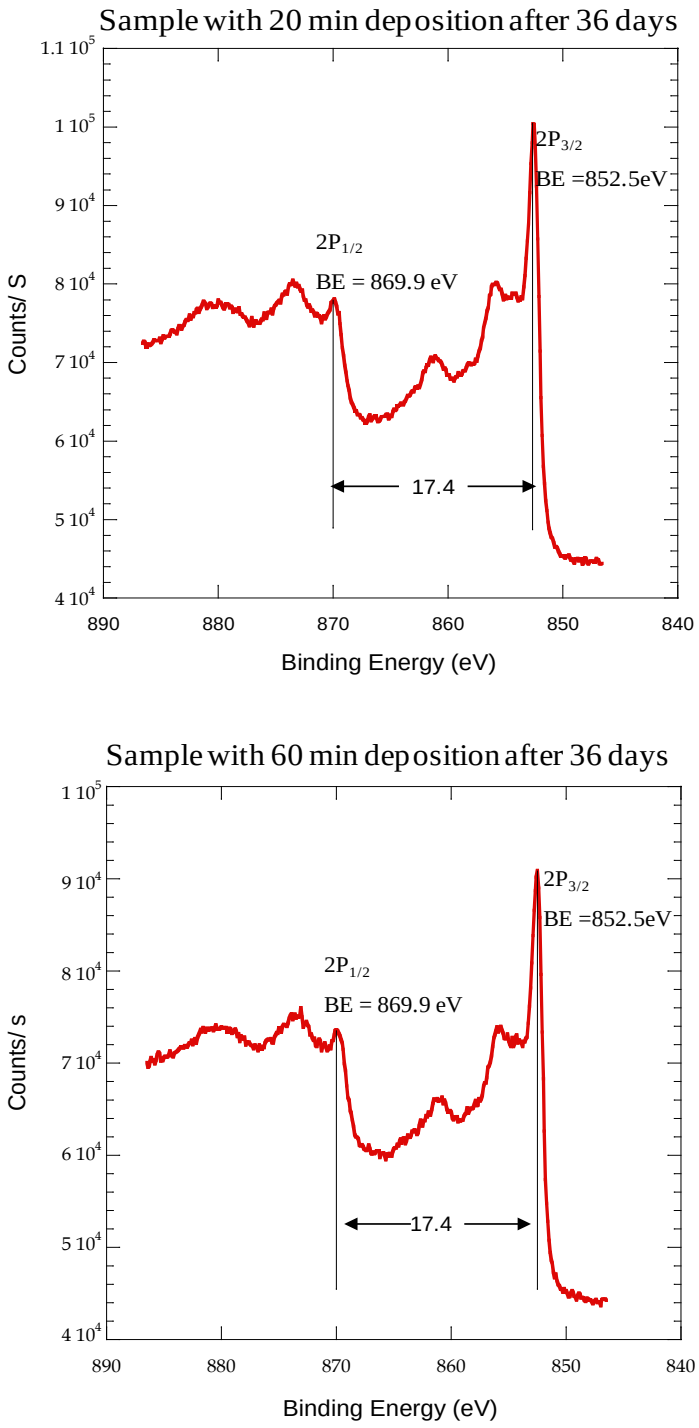

Fig 5.2 (b): XPS Core-level spectra of Ni2p after 36 days of samples with a 20 min and 60 min deposition time.

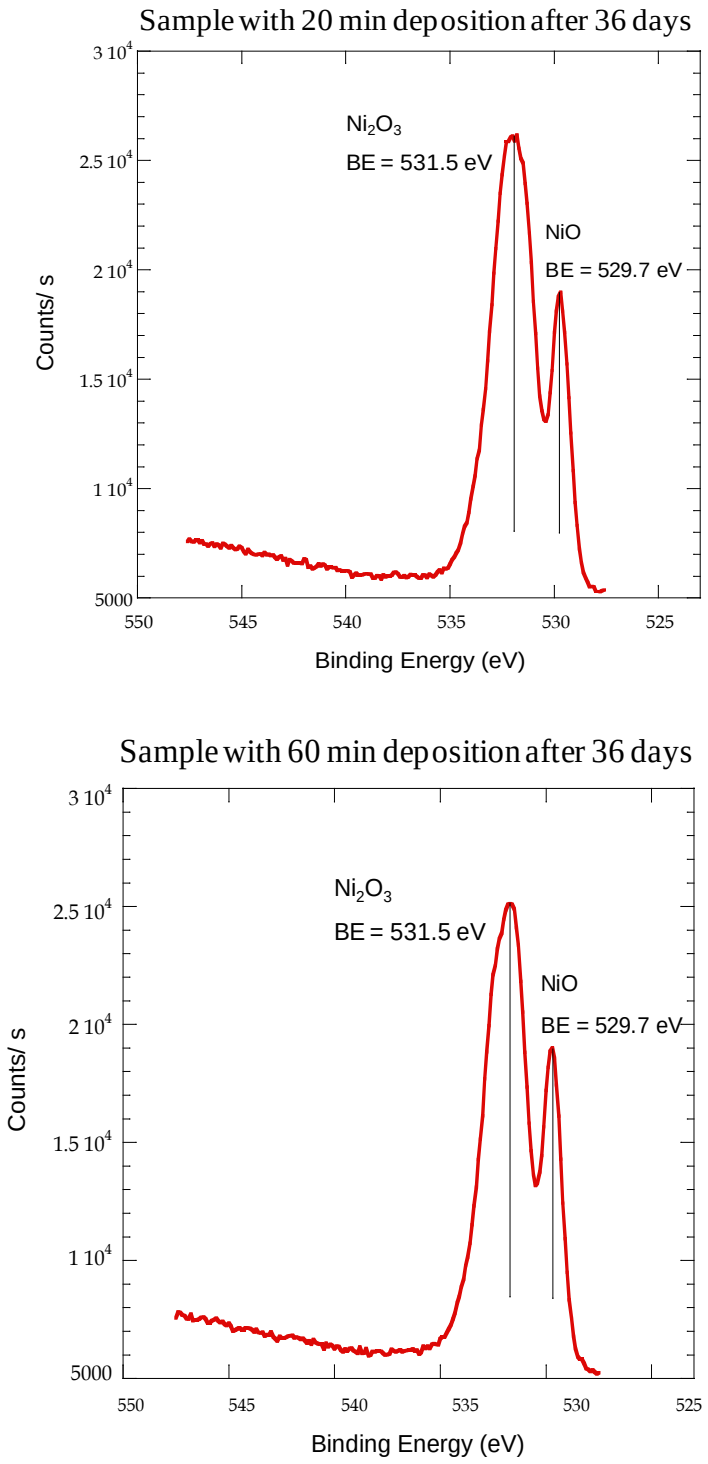

Fig 5.2 (c): XPS Core-level spectra of O1s after 36 days of samples with a 20 min and 60 min deposition time.

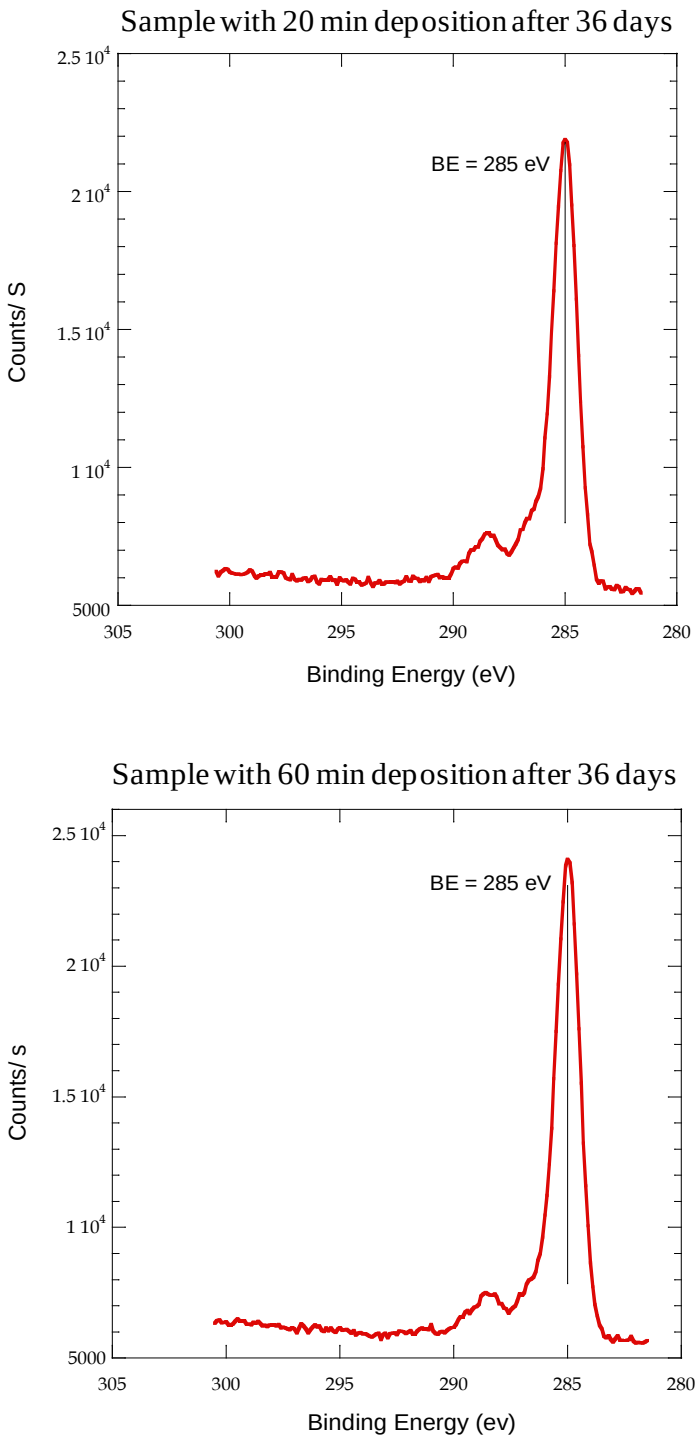

Fig 5.2 (d): XPS Core-level spectra of C1s after 36 days of samples with a 20 min and 60 min deposition time.

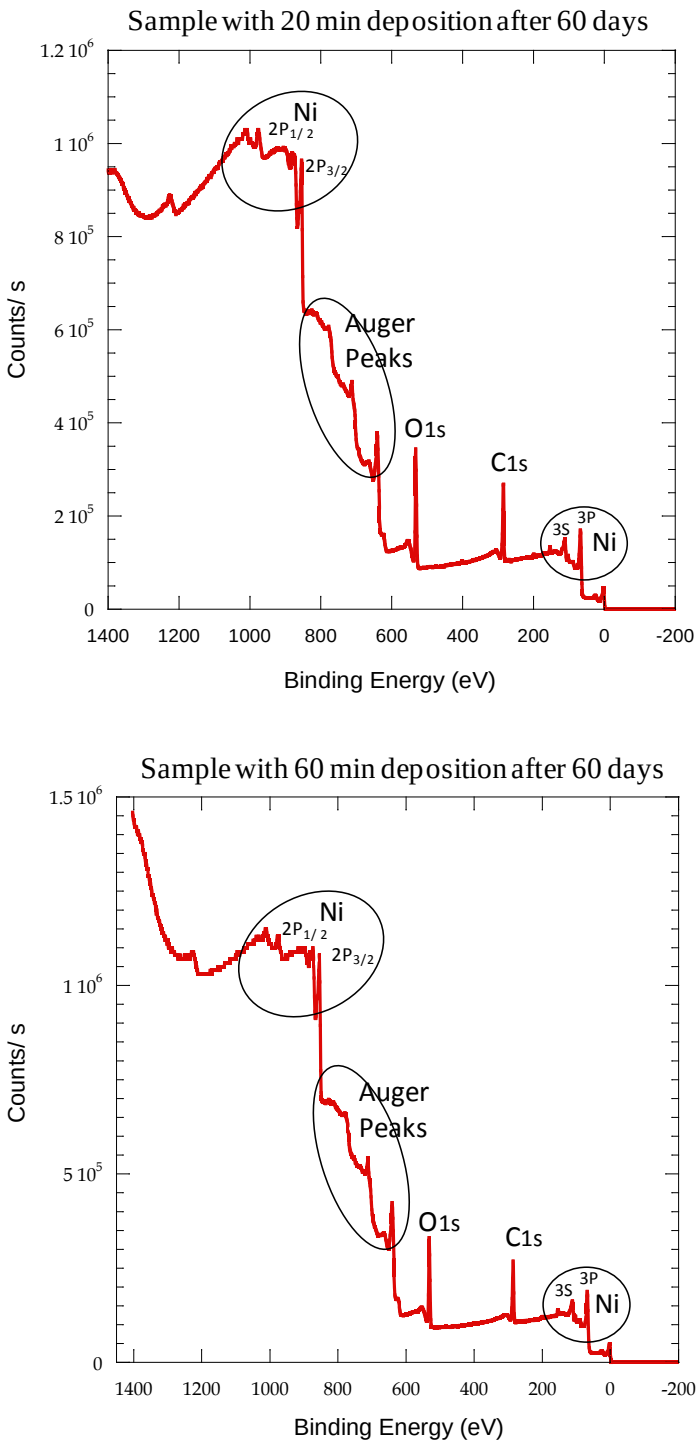

Fig 5.3 (a): XPS Survey spectrum after 60 days of samples with a 20 min and 60 min deposition time.

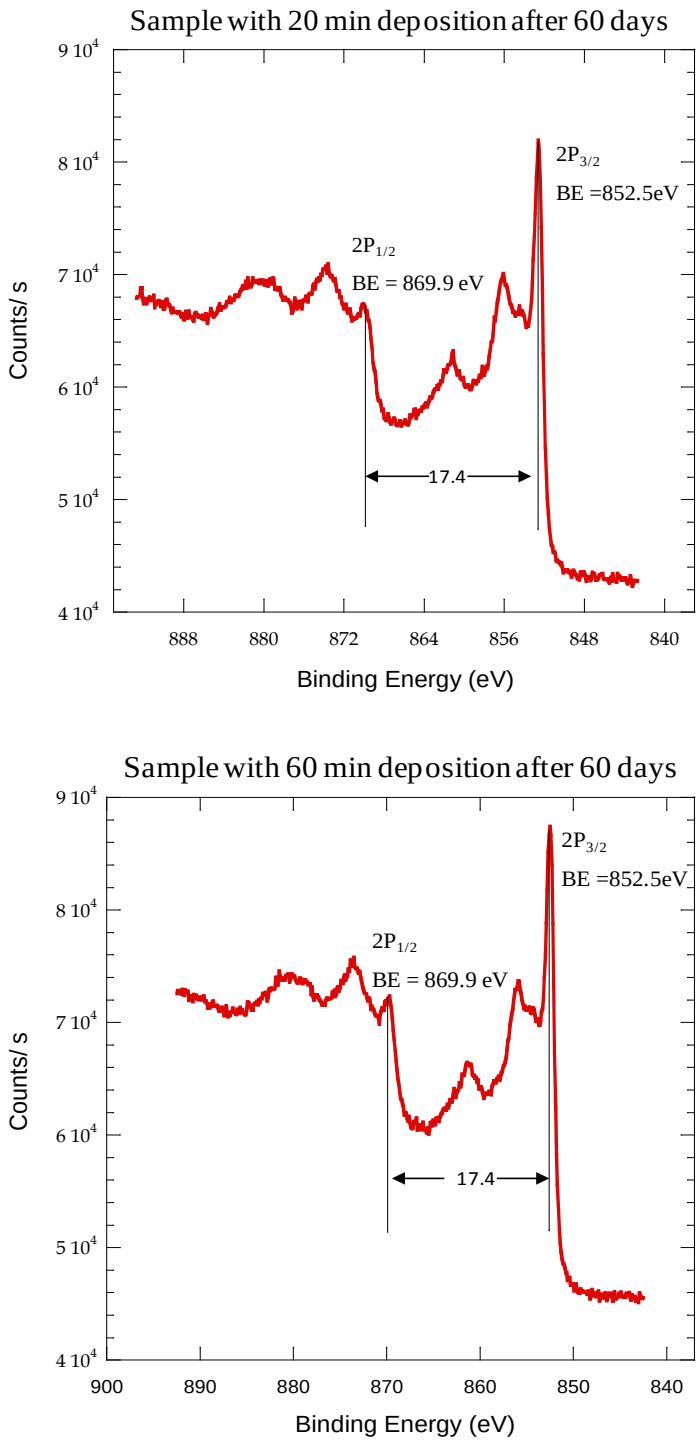

Fig 5.3 (b): XPS Core-level spectra of Ni2p after 60 days of samples with a 20 min and 60 min deposition time.

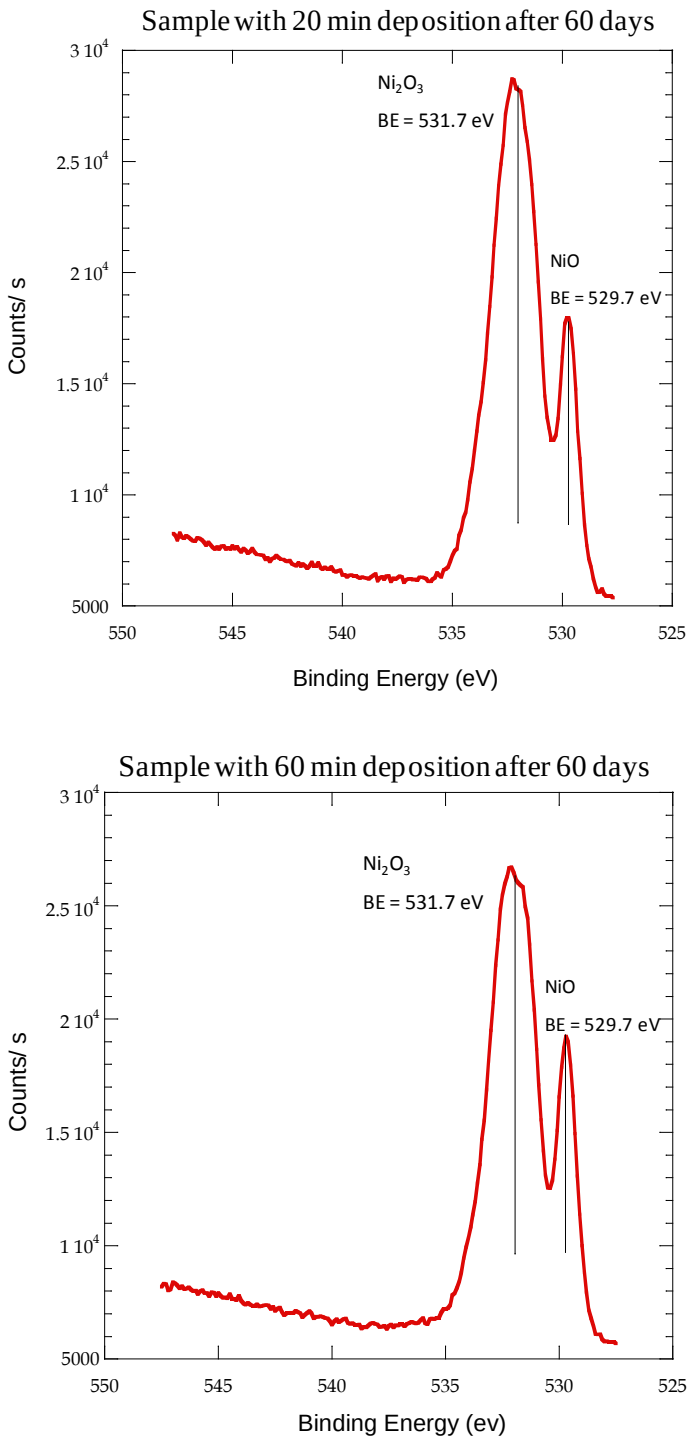

Fig 5.3 (c): XPS Core-level spectra of O1s after 60 days of samples with a 20 min and 60 min deposition time.

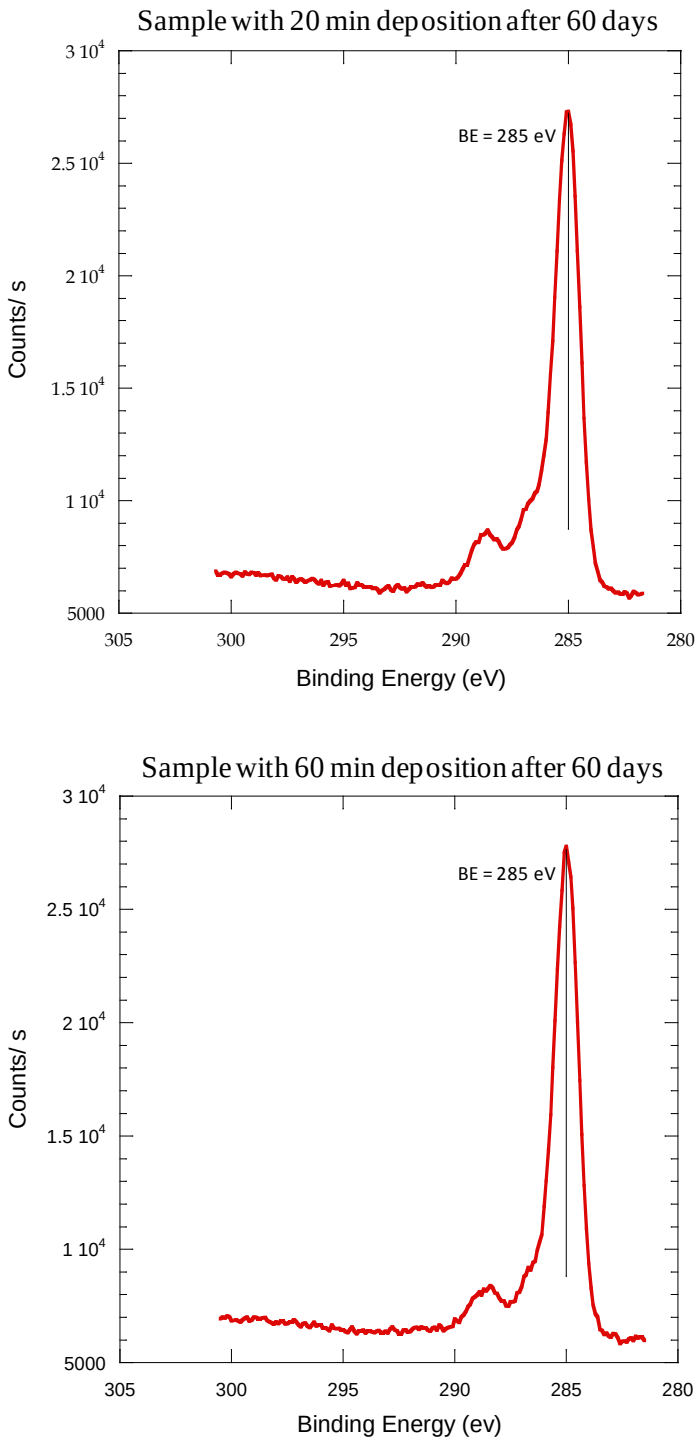

Fig 5.3 (d): XPS Core-level spectra of C1s after 60 days of samples with a 20 min and 60

Chapter 6: Conclusions and Future Work

The wettability has been studied for Ni nanorod samples by measuring the water contact angles in a period of aging time in air up to three months. The samples consisted of Ni nanorods arrays deposited on Si substrate by the dynamic oblique angle sputtering deposition technique. Each sample has different structural parameters, namely, the height and diameter of nanorods and the separation between them, which can be well controlled by the deposition time and the incident angle of atoms. From the SEM images, we observed that an increase in the structural parameters corresponded with the increase of deposition time. For example, the nanorods of samples with 20 minute deposition times were higher than those of samples with 10 minute deposition. Wetting experiments carried out immediately after deposition (approximately 30 minutes after breaking vacuum) showed that water on these samples completely wets the surface, giving contact angles less than 10°. The water contact angles increased over aging time as the samples were exposed to air. We observed that the increase in the water contact angles falls into two different groups. The samples with 10, 20, 30, 45, 50 and 55 minutes deposition time have larger increasing rates. The contact angles also changed from hydrophilic to hydrophobic during the duration of our experiment. In contrast, the samples prepared at 60 and 90 minutes have small increasing rates and remain hydrophilic during the same period of aging time in air.

It seems that the change of the water contact angles is a function of aging time and height of the nanorods. Since the water contact angle measurements are the same for all the samples right after the deposition, there is no immediate relationship between the morphology and the water contact angle. The effect of the morphology on the water contact angles comes at a later aging time when the nanorods react with air long enough, which causes an increase in the water contact angles. From XPS analysis, an increase of carbon species was observed with aging time in air. It is possible that the presence of the carbon could reduce the surface energy then decrease the adhesive force that is between the water and nanorods; however the thinner samples (10, 20, 30, 45, 50 and 55 minutes deposition time) adsorbed the carbon more than the thicker samples (60 and 90 minutes

deposition time), which caused the thinner samples to have a higher contact angle than the thicker samples.

We believe that the increase of water contact angles is due to the adsorbing of carbon species on the surface of the nanorods. To further investigate this mechanism, in future work, we will design the following experiments. First, hold the samples inside an ultra high vacuum environment for a period of aging time in air up to a couple of months. Multiple pieces of samples will be prepared by the same method with two different nanorod heights. We will pick up one of the samples from the vacuum chamber each aging time and take the water contact angles measurement and do the XPS analysis. Another method, After the samples gave a high water contact angles, we can put them again inside the ultra high vacuum for a couple of days then take the water contact angles measurements and do the XPS analysis again to compare the results. Second, expose carbon dioxide gas on the samples, and then leave them for a couple of days until they could adsorb it. After that, we will do other water contact angles measurements and XPS analysis and compare the results.

In future work, we will use different materials instead of nickel for the study of aging effects in water wettibility. It will be interesting to compare the results and find whether the water contact angles depend on the material properties of the nanorods.

References

[1]Wetting. (2011, April 29). In Wikipedia, The Free Encyclopedia. Retrieved 21:01, May 2, 2011, from http://en.wikipedia.org/w/index.php?title=Wetting&oldid=426595947

[2] P-G de Gennes, F. Brochard- Wyart, and D. Quere, *Capillarity and Wetting Phenomena*, Springer (2004)

[3] J.G. Fan, X.J. Tang and Y.P. Zhao, Nanotechnology **15**, 501 (2004)

[4] G.K. Kannarpady, R. Sharma, B. Liu, S. Trigwell, C. Ryerson, and A.S. Biris, Appl. Sur. Sci. **256**, 1679 (2010)

[5] B. Xu, Z. Cai, W. Wang, and F. Ge, Surf. Coat. Technol. **204**, 1556 (2010)

[6] R. N. Wenzel, Ind. Eng. Chem. **28**, 988 (1936)

[7] A. B. D. cassie and S. Baxter, Trans. Faraday Soc. **40**, 546 (1944)

[8] F. E. Bartell and P. H. Cardwell, J. Am. Chem. Soc. **64**, 494 (1942)

[9] D. J. Trevoy and Hollister Johnson, JR., J. Phys. Chem. **62**, 833 (1958)

[10] K. Robbie and M. J. Brett, J. Vac. Sci. Technol. A **15**, 1460 (1997)

[11] I. Safi, Surf. Coat. Technol. **127**, 203 (2000)

[12] C. D. Wanger, W. M. Riggs, L. E. Davis, J. F. Moulder, and G. E.Muilenberg, Handbook of X-ray Photoelectron Spectroscopy, Perkin-Elmer Corp., Physical Electronics Division, Eden Prairie, Minnesota, (1979)

[13] M. N.-Gamo, H. Gamo, K. Nakagawa, and T. Ando, J. Electrochem. Soc., Website: http://www.electrochem.org/dl/ma/206/pdfs/0934.pdf, (2005)

[14] Z. Liangzhong, P. Chenghuang, Acta Metall. Sin. **2**, 133 (1989)

[15] H.-L. Chang, T.-R. Jeng, J.-P. Chen, W.-H. Yen, P. Yen, D. Huang, and J.-J. Ju, Jpn. J. Appl. Phys. **44**, 6109 (2005).

[16] B Sasi and K G Gopchandran, Nanotechnology **18**, 115613 (2007)

[17] V. Datsyuk, M. Kalyva, K. Papagelis, J. Parthenios, D. Tasis, A. Siokou, I. Kallitsis, and C. Galiotisa, Sci.dir. Carbon **46**, 833 (2008)

[18] D. A Shirley, Phys. Rev. **5,** 4709 (1972)

[19] M. Alvisi, M. Blome, M. Griepentrog, Vasile-Dan Hodoroaba, P. Karduck, M. Mostert, M. Nacucchi, M. Procop , M. Rohde, F. Scholze, P. Statham, R. Terborg, and Jean-Francois Thiot, Micros. Microa. **12**, 406 (2006)

[20] T.B Ghosh and M. Sreemany, Appli. Sur. Scie. **64**, (1993)

[21] Neal Fairly, CasaXPS Manual, Introduction to XPS and AES, Version 2.3.15 (2009)

[22] R Rangel, D H Galvan, E Adem, P Bartolo-Perez and M B Maple, Supercond. Sci. Technol. **11,** 550 (1998)